

Comparative petrology and metamorphic evolution of the Limpopo (South Africa) and Lapland (Fennoscandia) high-grade terrains

L. L. Perchuk^{1,2}, T. V. Gerya^{2,1}, D. D. van Reenen³, A. V. Krotov¹,
O. G. Safonov², C. A. Smit³, and M. Yu. Shur¹

¹Department of Petrology, Moscow State University, Moscow, Russia

²Institute of Experimental Mineralogy, Russian Academy of Sciences, Chernogolovka, Russia

³Department of Geology, Rand Afrikaans University, Johannesburg, South Africa

With 14 Figures

Received March 8, 1999;

revised version accepted September 17, 1999

Summary

Detailed studies of rocks from the Limpopo (South Africa) and Lapland (Kola-Fennoscandia) high-grade terrains were carried out in order to reveal similar geological and thermodynamic conditions in their formation. Both complexes (1) are situated between Archean greenstone belts, (2) are younger than the belts, (3) are bounded by crustal-scale shear zones, (4) have a similar intrusive-like (harpolith) geometry, and (5) show similar reaction textures that reflect both breakdown and growth of garnet in each high-grade terrain. Local mineral equilibria within the textures indicate their successive formation with cooling of the granulite facies rocks. Some of the textures in the metapelites must have resulted from the following reverse reactions: $Grt + Qtz \rightleftharpoons Opx + Crd$ and/or $Grt + Sil + Qtz \rightleftharpoons Crd$. Based on these data, both the decompression cooling P - T path and the near-isobaric cooling P - T path were deduced for each HGT. However the near-isobaric cooling P - T path is not a characteristic of the central zones of both complexes studied.

Similar structural framework of the high-grade terrains, similar morphologies (shapes of granulitic bodies), similar reaction textures developed in metapelites, and similar shapes of P - T paths suggest similarity in geodynamic history of both complexes.

Zusammenfassung

Vergleichende Petrologie und metamorphe Entwicklung der hochgradig metamorphen Terrains von Limpopo (Südafrika) und Lapland (Fennoscandia)

Eingehende Untersuchungen an Gesteinen aus den hochgradig metamorphen Terrains von Limpopo (Südafrika) und Lappland (Kola-Fennoscandia) sollen mögliche Ähnlichkeiten in den geologischen und thermodynamischen Bildungsbedingungen aufzeigen.

Beide Komplexe sind

1. zwischen archaischen Grüngesteinsgürteln gelegen
2. jünger als die Grüngesteinsgürtel
3. begrenzt durch Scherzonen von krustalem Maßstab
4. mit ähnlicher, intrusionsartiger (Harpolith) Geometrie und
5. mit ähnlichen Reaktionstexturen, die sowohl den Zerfall wie auch das Wachstum von Granat in hochgradigen Terrains erkennen lassen.

Lokale Mineralgleichgewichte innerhalb der Texturen weisen auf ihre schrittweise Bildung während der Abkühlung der granulitfaziellen Gesteine hin. Einige der Texturen in den Metapeliten gehen auf folgende reversible Reaktionen zurück: $Grt + Qtz \rightleftharpoons Opx + Crd$ und/oder $Grt + Sil + Qtz \rightleftharpoons Crd$. Diese Daten ermöglichten es, sowohl den P - T Pfad der Abkühlung bei Druckentlastung sowie den fast-isobaren P - T Pfad der Abkühlung für jedes HGT zu ermitteln. Der fast-isobare P - T Pfad der Abkühlung ist jedoch kein Charakteristikum der Zentralzonen beider Komplexe.

Ein ähnlicher struktureller Rahmen der hochgradigen Terrains, ähnliche Morphologien (Ausbildung der Granulitkörper), ähnliche Reaktionstexturen in Metapeliten und ähnliche P - T Pfade weisen auf Ähnlichkeiten der geodynamischen Entwicklungsgeschichte beider Komplexe hin.

Geological abbreviations

HGT high grade terrain, *GSB* greenstone belts, *CZ* Central Zone, *NMZ* North Marginal Zone, *SMZ* South Marginal Zone, *HRSZ* Hout River Shear Zone, *TB* Tanaelv Belt, *ZC* Zimbabwe Craton, *KVC* Kaapvaal Craton, *MB* Murmansk Block, *KB* Kola Central Block, *PC* Pechenga Complex, *IC* Inari Craton, *KC* Karelian Craton, *BC* Belomorian Complex of the KC, *TB* Tanaelv Belt, *NSZ* Northern Shear Zone. See Appendix 1 for isotopic ages.

Mineral symbols

Alm almandine; *And* andalusite; *Ap* apatite; *Bt* biotite; *Chl* chlorite; *Crd* cordierite; *Cum* cummingtonite; *En* enstatite ($MgSiO_3$); *Ep* epidote; *Fs* ferrosilite ($FeSiO_3$); *Ged* gedrite; *Grt* garnet; *Grs* grossular; *Hbl* hornblende; *Ilm* ilmenite; *Kfs* *K* feldspar; *Ky* kyanite; *Mag* magnetite; *OK* "orthocorundum" (Al_2O_3) as a fictitious end-member of orthopyroxene (*Aranovich* and *Podlesskii*, 1989); *Opx* orthopyroxene; *Phl* phlogopite; *Pl* plagioclase; *Prp* pyrope; *Qtz* quartz; *Ru* rutile; *Sc* scapolite; *Sil* sillimanite; *Sph* sphene; *Spl* spinel; *Zc* zircon.

Introduction

One of the main objectives of modern metamorphic petrology is to explain formation and evolution of metamorphic complexes within a geodynamic framework based on detailed comparative structural, geochronological and geothermobarometric investigations of the rocks. In the case of Precambrian

HGT located between GSB, crustal evolution of these closely related units is usually considered in terms of collisional models (e.g., *Harley*, 1989; *Thompson*, 1990), although the critically important relationships between the HGT and adjacent GSB are rarely discussed (e.g., *Perchuk* and *Gerya*, 1995; *van Reenen* and *Smit*, 1996; *Perchuk* et al., 1997; *Percival* et al., 1997). On the basis of extensive studies, we may outline the following:

- (1) In many cases, HGT are younger than their cratonic counterparts (e.g., *Kreissig* and *Holzer*, 1997; *Bibikova* et al., 1993).
- (2) Some HGT include the high-grade metamorphic equivalents of typical Archean greenstone lithologies (e.g., *Petrova* and *Levitskii*, 1984; *Perchuk*, 1989, 1991; *van Reenen* et al., 1992; *van Reenen* and *Smit*, 1996; *Kozlov* et al., 1990).
- (3) Geometry of the HGT bodies is similar to that of the intrusive bodies (e.g., *de Wit* et al., 1993; *Barbey* and *Raith*, 1991; *Pozhilenko* et al., 1997).
- (4) A HGT is normally bounded by regional shear zones developed after the GSB rocks; non-isobaric metamorphic zoning is developed in the zones located in between the HGT and cratons (e.g., *Roering* et al., 1992b; *Przhjalgovsky* and *Terekhov*, 1995; *Perchuk* et al., 1999b, this volume).
- (5) Isotopic ages of material from the HGT and regional shear zones are similar (e.g., *Kreissig* and *Holzer*, 1997; *Perchuk* and *Krotov*, 1998).

Taking into account the above data, we have carried out a comparative study of two complexes, the Limpopo and Lapland HGT, that appeared to be very similar in their geological settings, geometry and geodynamic evolution.

Geological settings

The Limpopo HGT

The Limpopo HGT of southern Africa is a classic Archean high-grade complex with an exposed outcrop area of about 700 km in length and about 300 km in width (Fig. 1). It represents a continuous crustal section from the low-grade, i.e. GSBs of the KVC (> 2750 Ma, *de Wit* et al., 1992; *Kreissig* and *Holzer*, 1997) in the south, across the Limpopo HGT (~ 2640 Ma, *Kreissig* and *Holzer*, 1997) into the ZC (> 2800 Ma, *Rollinson*, 1997) contacting tectonically the Zimbabwe GSB in the north. A large volume of published data deals with different aspects of the Limpopo HGT (*Barton* and *van Reenen*, 1992; *Barton* et al., 1983; *Berger* et al., 1995; *Bohlender* et al., 1992; *Harris* and *Holland*, 1984; *Hofmann* et al., 1998; *Holzer* et al., 1997; *Jaeckel* et al., 1997; *Kreissig* and *Holzer*, 1997; *McCourt* et al., 1992; *Miyano* et al., 1990; *Mkweli* et al., 1995; *Perchuk* and *Gerya*, 1995; *Perchuk* et al., 1996; *Robinson* and *du Toit*, 1981; *Ridley*, 1992; *Roering* et al., 1992a, b, 1995; *Rollinson*, 1993, 1997; *Rollinson* and *Blenkinsop*, 1995; *Tsunogae* et al., 1992; *van Schalkwyk* and *van Reenen*, 1992; *van Reenen* and *Smith*, 1996; *van Reenen* et al., 1990 etc.). The Limpopo HGT is traditionally subdivided into the South Marginal Zone, Central Zone, and North Marginal Zone (Fig. 1a). Both the SMZ and NMZ are thrust over the Kaapvaal and Zimbabwe cratons, respectively. The time of thrusting in the marginal zones is constrained by the emplacement of syntectonic granitoids into the D2 shear zones (e.g., *Van Reenen* et al., 1995) to a

minimum age of about 2627 Ma. The northern part of the KVC is characterized by the general northward-verging thin-skinned thrust system (D1) (*van Reenen and Smit, 1996*). Formation of this structure was affected by the superimposition of the southward-verging fault system (D2) and emplacement of the SMZ onto the KVC (Fig. 3). The superimposition of D1 and D2 resulted in distinctive structural discontinuities at the terrain boundary. The greenstone rocks are faulted and rotated in concordance with the steep northward-dipping terrain boundary, which separates the KVC and the Limpopo belt (*McCourt and van Reenen, 1992*). This style of deformation is in strong contrast with that of the SMZ. In the SMZ, the remnant greenstone assemblages form highly attenuated and deformed lenses in granite-gneisses and migmatite bodies (Fig. 1). In the course of exhumation of the Limpopo complex, the SMZ rocks moved upward and spread outward onto the KVC, causing local metamorphism of the KVC rocks adjacent to the granulites. Details of the sheared boundary between the Limpopo HGT and adjacent KVC is discussed in a second paper (*Perchuk et al., this volume*).

The contact of the NMZ with the Zimbabwe craton is characterized by similar relationships. Greenstone belts adjacent to the NMZ (Fig. 1) contain thick sequences of mafic schists. Greenstone equivalent metabasites in the NMZ show a marked reduction in the outcrop size in comparison with the greenstone belts. This suggests that they have been last deformed during the same event that produced the characteristic ENE structural trend of the NMZ (*Mkweli and Blenkinsop, 1995*). The syn- to post-dynamic metamorphism of the area suggests that both the NMZ and the Zimbabwe craton were affected by the same metamorphic event that accompanied thrusting of the NMZ over and onto the ZC about 2600 Ma.

Geophysical, structural and metamorphic data support a model that involves north-south-directed thrusting (D1) across the entire Limpopo complex (*Roering et al., 1992a; de Wit et al., 1992*). According to this model, the high-grade rocks were uplifted to shallow crustal levels and thrust onto the low-grade rocks of the two adjacent cratons. The granulites suffered decompression and subsequent retrograde metamorphism, while the low-grade greenstones underwent prograde metamorphism (*Roering et al., 1992b; Perchuk et al., 1996, this volume*). Although no structural evidence of the final stage of evolution of the Limpopo granulite belt has been found, this can be constrained by the age of intrusion of two igneous complexes. Cross-cutting post-tectonic satellite bodies of the Great Dyke (2460 Ma, *Ridley, 1992*) were emplaced into metabasites of the NMZ (Fig. 1) that preserve igneous mineralogy and chilled margins indicating intrusion into cool rocks at a shallow crustal level. The post-tectonic *subvolcanic* Palmietfontein felsic dykes intruded metapelites of the SMZ at about 2540 Ma (*Barton and van Reenen, 1992*). The thrusting in the NMZ related to the exhumation of the Limpopo granulite complex is restricted to 2627 ± 7 Ma (*Mkweli et al., 1995*).

The SMZ of the Limpopo HGT

In Fig. 1a, the SMZ looks like a huge separate block of the Limpopo HGT. In the south, the SMZ is separated from the Kaapvaal craton by the Hout River Shear Zone. The SMZ is composed of pyroxene-bearing tonalitic gneisses (the Baviaanskloof Gneiss) and metapelitic granulite intercalated with mafic and

ultramafic granulites and banded iron formation (BIF) of the supracrustal Bandelierkop Formation. The metapelites are volumetrically the most important rock types in the SMZ. The Baviaanskloof Gneiss is penetratively deformed and commonly migmatized. The Bandelierkop Formation is intruded by homogeneous igneous enderbites of the Matok Complex (*Bohlender et al., 1992*). Metapelitic granulites of the Bandelierkop Formation consist of quartz, plagioclase, hypersthene, garnet, biotite and cordierite, with less common perthitic K-feldspar, spinel, sillimanite and late kyanite (e.g., *van Reenen et al., 1990*). These rocks are coarsely banded and often migmatized. They preserve symplectitic reaction textures, which are similar to described rocks of the CZ (*van Reenen et al., 1990*) and the NMZ (*Tsunogae et al., 1992*). The leucocratic portion of the rocks is composed mainly of perthitic K-feldspar and plagioclase with minor graphite, sillimanite, garnet and cordierite. Mafic granulites are coarse-grained, foliated rocks, characterized by the assemblage $Pl + Opx + Cpx + Mag + Ilm + Hbl$. Banded iron formation is closely associated with both metapelites and metabasites. In mineral composition these rocks vary from a banded rock ($Qtz + Mag + Opx$) to a more massive rock ($Qtz + Opx + Grt + Mag$). Ultramafic granulites are massive rocks composed of forsterite, spinel, enstatite and pargasitic hornblende (*van Schalkwyk and Van Reenen, 1992*). The isotopic age of the SMZ (Fig. 1) varies within relatively narrow limits, 2691–2637 Ma (*Kreissig and Holzer, 1997*).

The CZ of the Limpopo HGT

The CZ is mainly characterized by a unique shelf-type supracrustal succession (different metapelites, metabasites, BIF, and metalimestones) intruded by a layered igneous complex. The CZ is separated from the marginal zones by inward-dipping mylonitic shear zones with strike-slip characteristics. In contrast, both marginal zones are separated from the adjacent GSB by inward-dipping thrust zones. The Pb-Pb dating of metamorphic sillimanite (2573 ± 15 Ma, *Holzer et al., 1998*) and single metamorphic zircons (2575 ± 4 Ma, *Kröner et al., 1998*) defines a high-grade metamorphic event in the CZ (Fig. 1). This age (2570 Ma) is slightly younger than that of the SMZ. The difference in age is probably related to a longer cooling time of the CZ under static metamorphic conditions (*Hofmann et al., 1998*), or a late metamorphic event (i.e., hydration of cordierite). Numerous granitic bodies with ages around 2600 Ma occur in the CZ (*Kröner et al., 1998*). Large metapelitic blocks in the CZ experienced strong hydrothermal alteration (*van Reenen et al., 1990*). This event is presumably reflected in the younger U/Pb isotopic age (about 1900–2000 Ma, *Holzer et al., 1997*) of zircons from the altered metapelites.

The NMZ of the Limpopo HGT

The NMZ is composed of three major groups: (1) a dominant plutonic assemblage composed of large volumes of charnockitic rocks, (2) porphyritic granites emplaced into a minor supracrustal assemblage, and (3) mafic granulites, BIF and amphibolites (*Rollinson and Blenkinsop, 1995*). Charnoenderbites of group (1) form narrow bands in tonalitic gneisses and large relatively homogeneous bodies (*Robinson and du Toit, 1981; Ridley, 1992; Berger et al., 1995*). The assemblage

$Pl + Opx + Qtz + Kfs + Bt$ with minor clinopyroxene, hornblende and garnet is the most widespread in the rocks. Porphyritic potassium-rich granites of group (2) constitute the so-called Razi suite (Robinson, 1973, 1974) that intruded the NMZ–CZ D2 shear boundary over a strike-length of about 100 km. The rocks of group (3) reflect a typical supracrustal greenstone lithology and occupy about 10% of the exposed area in the NMZ. Mafic granulites of the group consist of orthopyroxene, clinopyroxene, plagioclase and pargasitic hornblende. Greenstone lithologies also include rare metapelites, quartzites and marbles. The metapelites are characterized by decompression-related cordierite coronas developed around the $Grt + Sil + Qtz$ assemblage (Tsunogae et al., 1992). Mafic and ultramafic layered complexes, including serpentinites and metapyroxenites (Rollinson and Blenkinsop, 1995), are intimately associated with metasediments and metabasites. The ultramafic gneisses are composed of pargasitic hornblende, orthopyroxene and clinopyroxene.

The isotopic age of the NMZ (Fig. 1) is similar to that of the SMZ. According to Jaeckel et al. (1997), granulite facies conditions in the NMZ occurred between 2620 and 2580 Ma. This age is verified by dating of six syntectonic enderbite-charnoerbite bodies (Fig. 1), whose age varies between 2580 and 2710 Ma (Berger et al., 1995). Kamber and Biino (1995) suggest that the magmatic activity in the NMZ is manifested by the emplacement of charnoenderbites, porphyritic granites and charnockites with ages between 2700 Ma and 2580 Ma. The thrusting in the NMZ, related to the exhumation of the Limpopo granulite complex is restricted to 2627 ± 7 Ma (U-Pb zircon age), i.e. to the emplacement of the porphyritic Razi granite suite into the D2 shear zones (Mkweli et al., 1995).

The Lapland HGT

The Lapland HGT in the northern part of the Baltic shield forms a 50–100 km wide arc from the Caledonides in the north to the Early Proterozoic Kola series of acid and basic granulites (Fig. 2). In terms of the geological structure and rock composition, the Lapland HGT can be divided into two non-equivalent portions (Mints et al., 1996). The western portion of the Lapland HGT has been studied over a long time period (Eskola, 1952; Mikkola, 1937, 1941; Merrillainen, 1976; Hörmann et al., 1980; Barbey et al., 1980, 1984; Bersthelsen and Marker, 1986; Barbey and Raith, 1990; Bernard-Griffiths et al., 1984; Gaal et al., 1989; Krill, 1985; Marker, 1988, 1990, 1991 etc.), while the eastern portion has been studied mainly during the last twenty years (Latyshev, 1971; Vinogradov et al., 1980; Kozlov et al., 1990; Bogdanova and Daly, 1991; Mints et al., 1996; Bibikova et al., 1993; Glebovitskiy et al., 1996; Bogdanova and Efimov, 1997; Perchuk and Krotov, 1998; Perchuk et al., 1999a etc.).

Tectonically, the 1900 Ma Lapland HGT resembles a huge horseshoe structure or a nappe bounded by thrusts on both sides. Seismic data (Marker, 1988, 1991; Pozhilenko et al., 1997) show that the thrusts are semi-parallel and, thus, suggest that the Lapland granulite body is very similar in shape to a harpolith¹ (Fig. 3). Both the Karelian Craton and the Inari Craton, juxtaposed against the Lapland belt,

¹ Harpolith is a large sickle-shaped igneous intrusion injected into previously deformed strata (Glossary of Geology, 1997; Gary et al., 1972; Tomkeieff, 1983).

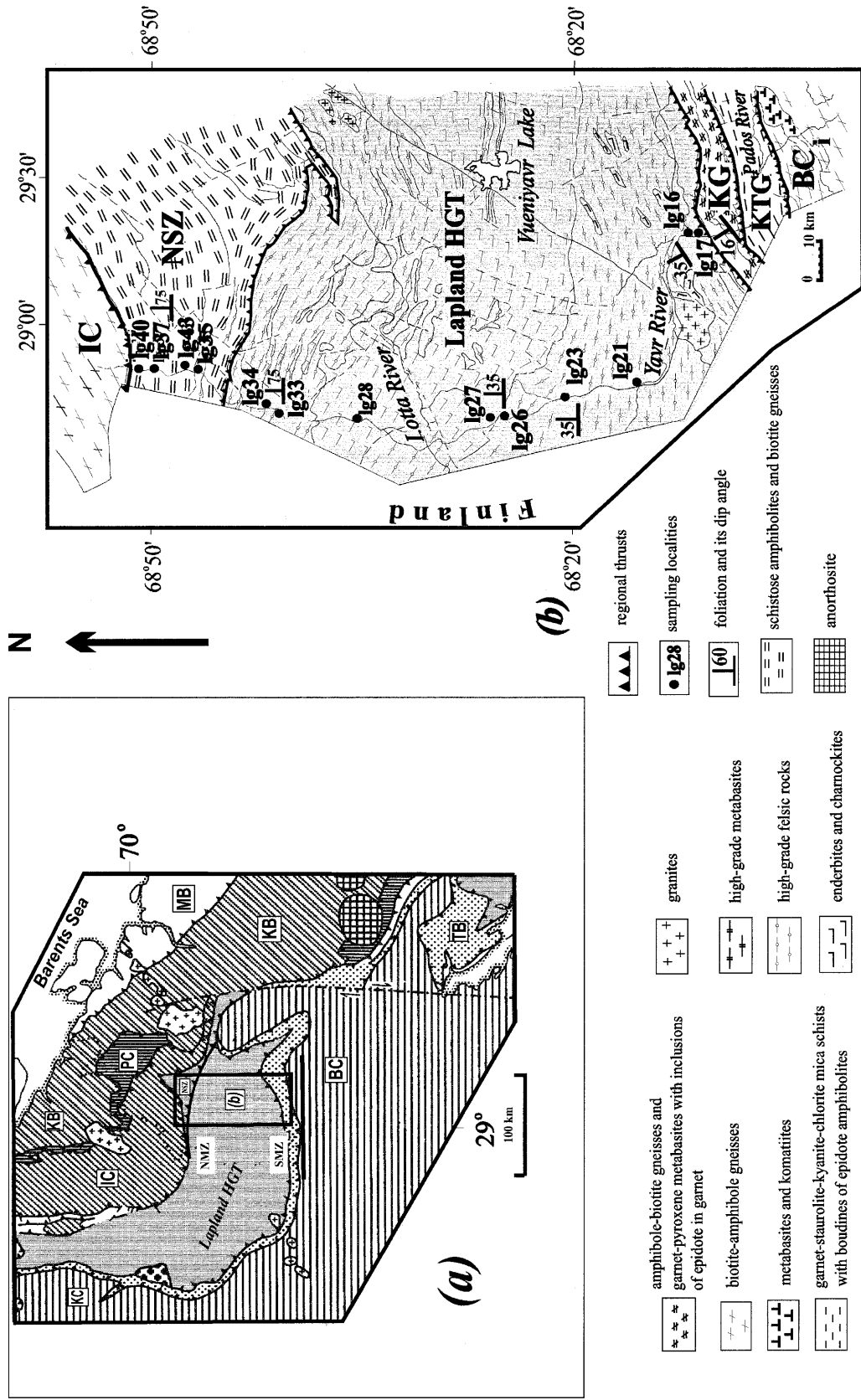


Fig. 2. Geological maps of the Lapland area. The NMZ and SMZ in **a** indicate the North Marginal Zone and the South Marginal Zone, respectively

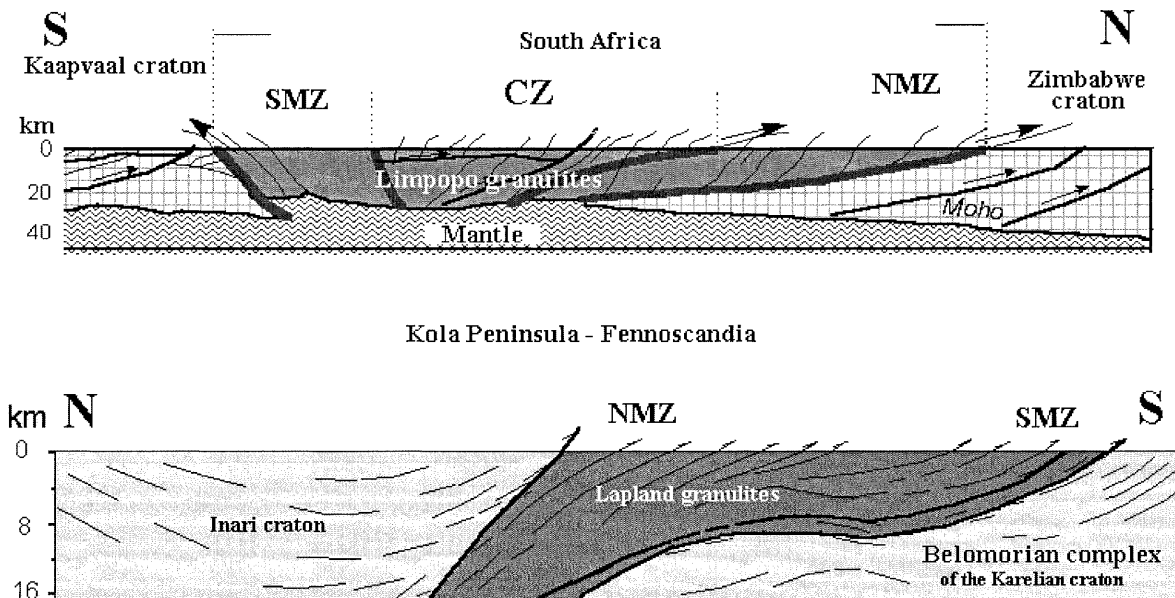


Fig. 3. Cross-sections of the Limpopo and Lapland HGTs based on integrated structural, geological and seismic data (*van Reenen and Smit, 1996; Pozhilenko et al., 1997; Marker, 1990*)

show isotopic ages older than ~ 2500 Ma (*Merillainen, 1976; Bibikova et al., 1993*). The Lapland HGT is underlain by the Tanaelv Belt (Fig. 2). The latter forms an intensely sheared thrust belt dipping gently NE and composed of low-grade to granulite-facies rocks of different ages (2460–2050 Ma) and compositions (*Marker, 1991; Mitrofanov et al., 1993; Mints et al., 1996; Bogdanova and Efimov, 1997; Perchuk et al., 1999a*). Between 1950 and 1750 Ma, both the Lapland and the Tanaelv belts were intruded by plutonic rocks of various compositions (*Barbey et al., 1984; Bernard-Griffiths et al., 1984; Krill, 1985*), mostly granitoids (*Mints et al., 1996*), which indicate that the Lapland HGT is younger than the wall rocks. In direct contact with the granulites their primary isotopic age has been rejuvenated due to the thermal effect.

According to the deformation style, the Lapland HGT can be subdivided into two units: unsheared anatectic rocks located in the NE portion of the nappe structure and strongly sheared high grade rocks of the SSW side of the granulite body. According to *Marker (1991)*, the anatectic metasediments show a high degree of partial melting with irregular patterns of neosome veins grading into almost nebulous rock types. Towards the underlying sheared granulites, the neosome gradually attains a pronounced parallel planar structure due to an increase in the shear strain. The shear strain likely increased towards the southern and southwestern parts of the nappe, where the granulites were transformed into well-developed mylonites. The mylonite shows a strong penetrative foliation characterized by platy quartz and sheared neosomes with the development of thin leucocratic bands. This fine-grained planar foliated rock dips gently to the north-

north-east, indicating thrusting to the south-south-west. Cordierite does not occur in the mylonitic granulites, while garnet and feldspar often form augen-shaped porphyroblasts. Boudins of enderbite gneiss after meta-igneous rocks are developed in the metasediments (e.g., *Barbey and Raith, 1990*). The gneisses also show scattered and diffused neosomes composed of plagioclase, orthopyroxene, and/or hornblende. The rocks occur as thin elongated bodies parallel to the mylonitic foliation. Metabasic boudins are likewise mylonitized producing a rock of distinct planar mylonitic character (*Marker, 1991*).

Petrographically, rocks of the Western zone can be subdivided into three series: (1) khondalites, (2) enderbites, and (3) migmatite-kinzigite series (*Eskola, 1952; Barbey and Raith, 1990*). The first series forms a major component of the belt and consists of intimately banded and foliated gneisses with rare bands and boudins of $Opx + Bt + Grt + Pl + Qtz$ gneisses and calc-silicate rocks. Rocks of the enderbite series form complementary bands, dykes and intrusive bodies among the metasediments, while cores of enderbite preserve primary magmatic textures. The third series (anatectic portion of the Lapland belt in Fig. 2) is characterized by the partial melting of sillimanite-garnet and garnet-bearing gneisses, where the leucosomes correspond to the granitic minimum in terms of the $Qtz:Pl:Kfs$ ratio, while the restite is a typical kinzigite ($Bt + Grt + Sil + Crd + Qtz + Kfs + Pl + Spl$).

In contrast to Fennoscandia, the Eastern portion of the Lapland granulite belt, at the northern coast of the Kandalaksha gulf, White Sea, contains metamorphic enderbites, metagabbro, gabbro-norite, and gabbro-anorthosite bodies. The cores of

Table 1. *U-Pb ages of rocks from the Lapland and Limpopo HGT, shear zones, and adjacent cratons*

Rock	Zone/Group	Age, Ma	Reference
Lapland area			
Kyanite-bearing mica schist	Western part of the Tanaelv belt (Finland)	1900	<i>Bernard-Griffiths et al. (1984)</i>
Kyanite-bearing mica schist	Korva Tundra group of the Tanaelv belt (Russia)	1910	<i>Volodichev (1990)</i>
Granulitic gneiss	Southern part of the Lapland HGT	1916	<i>Bibikova et al. (1993)</i>
Gray gneisses	Belomorian Complex of the Karelian Craton	> 2700	<i>Kozlov et al. (1990)</i>
Limpopo area			
Kyanite-bearing schist	Hout River shear zone, at the contact with granulite body	2689	<i>Kreissig and Holzer (1997)</i>
Granulitic metapelite	South Marginal Zone	2691	<i>Kreissig and Holzer (1997)</i>
Charnoenderbite	Matok pluton located in the SMZ	2671	<i>Barton et al. (1992)</i>
Metavolcanics	Kaapvaal Craton	> 2750	<i>de Wit et al. (1992)</i>

these bodies preserve igneous textures, while their margins are strongly deformed and metamorphosed under granulite-facies conditions. The eastern end of the Lapland HGT is presented by the Main Ridge Zone (8–10 km wide) composed of basic meta-igneous rocks, which record a very long and complex geological history. According to numerous isotopic data (*Bogdanova and Efimov, 1997*), ages of orthogneisses from this area vary between 1.88 and 2.2 Ga, while the emplacement of gabbro-anorthosites is dated at about 2.46–2.4 Ga (e.g., *Mitrofanov et al., 1993; Frisch et al., 1995*) which is significantly different from that of the Lapland HGT (~1.9 Ga).

Table 1 summarizes isotopic ages of major metamorphic events in different units of the Limpopo and Lapland areas. These data show that the HGT and GSB differ in age. The rocks from the contact sheared zones composed of GSB material must have been re-equilibrated in terms of *P-T* conditions, and their isotopic ratios may reflect the HGT emplacement ages.

Petrology

Petrographic descriptions of the different rock types from both the Limpopo HGT (e.g., *van Reenen et al., 1990*) and the Lapland HGT (e.g., *Eskola, 1952; Barbey and Raith, 1990*) were repeatedly given by many workers. The rocks of both complexes are similar in their bulk and mineral compositions, reaction textures etc. Moreover, distributions of metabasites, metapelites, and felsic gneisses within the Lapland and Limpopo HGT are also similar.

For example, metabasites are restricted to the margins of both bodies. Metabasites from the Lapland HGT are well studied (*Raith and Raase, 1982; Barbey and Raith, 1990; Daly and Bogdanova, 1991; Fonarev et al., 1994*), but their *P-T* evolution has not yet been considered. In contrast to the Lapland complex, the Limpopo HGT metapelites are more abundant and thoroughly investigated. Although various rock types from both complexes contain well-developed reaction textures, metapelites allow a more thorough study of the *P-T* evolution of the rocks.

The geodynamic regime of a metamorphic complex is known to be recorded in its *P-T* path (*Perchuk, 1973, 1977, 1989, 1991; Perchuk et al., 1996*). The *P-T* paths were also discussed by many workers for both areas under consideration (e.g., *Daly and Bogdanova, 1991; Fonarev et al., 1994; Hisada and Miyano, 1996*). However, the path shape may be different for different complexes and may greatly depend on the mechanism operating during the course of emplacement of a given metamorphic complex.

Petrographic study of the rocks was accompanied by microstructural analysis, and microprobe data were used to calculate the *P-T* parameters from the compositions of coexisting minerals in each given rock sample. Mineral assemblages of the rocks studied with the microprobe are presented in Table 2. Examples that illustrate how the *P-T* parameters can be deduced from reaction textures and mineral zoning and then used to interpret the thermodynamic and geodynamic evolution are provided in Appendix 2.

As demonstrated in earlier studies (*Perchuk et al., 1996; Gerya et al., 1997*), exchange and net-transfer reactions, if considered together, allow simultaneous

Table 2. *Representative mineral assemblages used for thermobarometry*

Sample, No	Mineral assemblage	Microprobe* store
Limpopo HGT (Fig. 1b)		
LW7	<i>Grt + Crd + Opx + Bt + Qtz + Pl + Spl</i>	1–54, G1–G51, C1–C62
DV3	<i>Grt + Crd + Opx + Qtz + Pl + Sil/Ky + Ged + Cum + Bt</i>	B7–B57
R8	<i>Grt + Crd + Opx + Qtz + Pl + Bt + Sil/Ky + Ged + Cum</i>	X1–X66
DV101	<i>Grt + Crd + Opx + Bt + Qtz + Pl + Sil</i>	B1–B45
DR45	<i>Grt + Crd + Opx + Bt + Qtz + Pl</i>	A1–A60
DR19	<i>Grt + Crd + Opx + Qtz + Pl + Kfs + Bt + Sil + Spl</i>	63–127
DV81	<i>Grt + Crd + Opx + Bt + Qtz + Pl + Sil</i>	11–184
BY27	<i>Grt + Crd + Opx + Bt + Qtz + Pl</i>	D1–D62
BY30	<i>Grt + Crd + Sil + Bt + Qtz + Pl + Spl</i>	Z1–Z43
Lapland HGT (Fig. 2b)		
KL1098	<i>Grt + Crd + Opx + Bt + Qtz + Pl</i>	1–56
lg-16/5	<i>Grt + Opx + Bt + Qtz + Pl + [Sc + Zc]</i>	1–37
lg-17/1	<i>Grt + Opx + Cpx + Hbl + Qtz + Pl</i>	1–59
lg-16/1	<i>Grt + Bt + Pl + Qtz + Kfs + [Sil + Zc + Ru]</i>	1–44
lg-23	<i>Grt + Bt + Pl + Qtz</i>	4–20
lg-33	<i>Grt + Bt + Sil + Crd + Qtz + Pl + Kfs + [Zc + Ru + Ilm]</i>	1–15
lg-34	<i>Grt + Bt + Sil + Crd + Qtz + Pl + Kfs + [Zc + Ru + Ilm + Sph]</i>	8–126

*Probe analyses are available from the authors on e-mail request

calculation of P and T from composition of coexisting minerals. For example, the assemblage $Grt + Opx + Crd + Qtz$ can be considered as formed due to reactions r2–r5 of Table A2-1 in Appendix 2, while reactions r1 and r2 can describe the formation of reaction textures in the assemblage $Grt + Crd + Sil + Qtz$. Practically, T can be calculated with the Crd - Grt thermometer (exchange reaction r2 of Table A2-1 in Appendix 2), while P is calculated from the net-transfer reactions (r1 or r5 of Table A2-1 in Appendix 2).

The thermodynamic data of Table A2-1 in Appendix 2 are taken from the data set created for an internally consistent system of geothermometers and geobarometers (Perchuk et al., 1985; Aranovich and Podlesskii, 1989; Gerya and Perchuk, 1990). Based on these data, isopleths for the above mineral assemblages

were computed by solving the systems of independent thermodynamic equations for simultaneously operating reactions, and this allowed visual tracing of the composition evolution of coexisting minerals as a function of P and T . The water activity in a fluid was calculated using thermodynamic data for reactions r7 and r9 from Table A2-1 in Appendix 2.

Derivation of a P - T path for each given sample involved four major steps:

- (1) Definition of the formation sequence of the reaction microtextures.
- (2) Definition of the chemical evolution of the texture-forming minerals on the basis of microprobe analyses. Diffusion profiles for the contacting Fe-Mg minerals were studied in order to distinguish between exchange and net-transfer mechanism of the reactions.
- (3) Calculation of P - T parameters for different stages of the formation of the reaction textures. A standard “core-core \Rightarrow rim-rim” method was used for each given generation of a reaction texture.
- (4) Derivation of P - T trajectory related to the composition isopleths for divariant assemblages.

At step (4), bulk compositions of the samples (Table A2-3 in Appendix 2) were used to calculate garnet isolines in the P - T diagrams by solving the system of thermodynamic equations for the observed $Grt + Opx + Crd + Qtz$ and $Grt + Sil + Crd + Qtz$ reaction textures formed after reactions r2–r5 and r1–r2 in Table A2-1 in Appendix 2, respectively coupled with mass-balance equations for components Si' , Al' , Mg' and Fe' (Gerya, 1991). These components were estimated from the bulk rock composition as follows (in atomic percents): $Si' = Si - 2Ca - 3Na - 3K$, $Al' = Al - 2Ca - Na - K$ (a correction for the Si-Al content in feldspars), $Mg' = Mg$ and $Fe' = Fe^{2+} + Fe^{3+}$ (all iron was assumed to be divalent). In the P - T field, isopleths of the garnet content in a rock were standardized to a conventional granulite containing garnet as the only mafic mineral. Being aware of the limitations of the calculations, we assume that they reflect changes in the garnet content in a real rock with changing P and T .

Examples of derivation of the P - T path for samples DR45 and DR19 are given in Appendix 2. Compositions of coexisting minerals in these samples and calculated P - T parameters of the mineral equilibria are given in Table 3.

Reaction textures in metapelites

Two principal metapelitic assemblages were studied in samples from the Limpopo and Lapland complexes: $Grt + Crd + Opx + Qtz + Pl$ and $Grt + Crd + Sil + Qtz + Pl$. The following three types of reaction textures were observed in both assemblages:

- I. Reaction textures reflecting a decompression-cooling history. These are: Crd - Opx coronas developed between garnet and quartz due to the reaction $Grt + Qtz \Rightarrow Crd + Opx$ (Fig. 4a, b); cordierite coronas around garnet resulted from the reaction $Grt + Sil + Qtz \Rightarrow Crd$.
- II. Reaction textures reflecting an isobaric-cooling history. These are: small euhedral garnet crystals filled with inclusions of sillimanite formed after

Table 3. *Molar fractions* of some components in coexisting minerals from metapelites and calculated P-T parameters** for samples from the SMZ of the Limpopo HGT*

<i>Grt</i> Spot	X_{Mg}	X_{Ca}	X_{Mn}	<i>Opx</i> Spot	X_{Mg}	X_{Al}	<i>Crd</i> Spot	X_{Mg}	<i>T</i> , °C	<i>P</i> , kbar
DR45 (cores)										
a29	0.467	0.026	0.005	a59	0.683	0.075	a43	0.841	746	6.42(r5)
a30	0.475	0.024	0.006	a57	0.679	0.069	a56	0.843	752	6.59(r5)
a31	0.471	0.029	0.004	a44	0.674	0.064	a43	0.841	752	6.53(r5)
a12	0.508	0.049	0.008	a59	0.683	0.075	a43	0.841	808	7.35(r5)
a13	0.508	0.050	0.006	a59	0.683	0.075	a43	0.841	808	7.35(r5)
a14	0.510	0.052	0.009	a59	0.683	0.075	a43	0.841	811	7.40(r5)
a15	0.497	0.049	0.006	a59	0.683	0.075	a43	0.841	790	7.10(r5)
a0	0.523	0.063	0.003	a59	0.683	0.075	a43	0.841	832	7.71(r5)
a1	0.514	0.060	0.006	a59	0.683	0.075	a43	0.841	817	7.49(r5)
a2	0.511	0.054	0.006	a59	0.683	0.075	a43	0.841	812	7.42(r5)
a3	0.513	0.057	0.008	a59	0.683	0.075	a43	0.841	816	7.47(r5)
a4	0.488	0.048	0.006	a59	0.683	0.075	a43	0.841	777	6.89(r5)
a5	0.496	0.048	0.004	a59	0.683	0.075	a43	0.841	789	7.08(r5)
a6	0.479	0.041	0.005	a59	0.683	0.075	a43	0.841	763	6.69(r5)
DR45 (rims)										
a28	0.418	0.026	0.012	a54	0.678	0.046	a27	0.845	671	5.22(r5)
a32	0.438	0.027	0.006	a35	0.685	0.043	a36	0.844	698	5.53(r5)
a33	0.433	0.032	0.008	a34	0.676	0.047	a37	0.850	679	5.55(r5)
a40	0.422	0.033	0.010	a38	0.672	0.046	a39	0.852	661	5.36(r5)
a41	0.424	0.028	0.010	a38	0.672	0.046	a42	0.841	687	5.41(r5)
a49	0.394	0.028	0.008	a54	0.678	0.046	a53	0.848	635	4.72(r5)
a50	0.404	0.033	0.010	a54	0.678	0.046	a53	0.848	647	4.93(r5)
a50	0.404	0.033	0.010	a54	0.678	0.046	a52	0.862	618	4.93(r5)
a51	0.394	0.034	0.013	a54	0.678	0.046	a52	0.862	607	4.73(r5)
DR19 (cores)										
70	0.393	0.029	0.009	–	–	–	77	0.840	655	5.65(r1)
71	0.399	0.025	0.011	–	–	–	76	0.832	679	5.86(r1)
72	0.394	0.027	0.013	–	–	–	78	0.832	673	5.78(r1)
96	0.403	0.026	0.012	–	–	–	104	0.839	669	5.83(r1)
97	0.406	0.027	0.014	–	–	–	105	0.835	681	5.93(r1)
122	0.395	0.028	0.013	–	–	–	104	0.839	692	5.94(r1)
123	0.394	0.027	0.012	–	–	–	104	0.839	659	5.68(r1)
124	0.395	0.026	0.011	–	–	–	105	0.835	688	5.88(r1)
125	0.399	0.026	0.012	–	–	–	105	0.835	673	5.82(r1)
DR19 (rims)										
81	0.395	0.018	0.009	–	–	–	85	0.846	645	5.58(r1)
82	0.380	0.027	0.015	–	–	–	100	0.842	636	5.40(r1)
83	0.396	0.030	0.009	–	–	–	100	0.842	654	5.66(r1)
84	0.388	0.020	0.005	–	–	–	99	0.861	605	5.22(r1)
93	0.393	0.016	0.013	–	–	–	85	0.846	643	5.55(r1)
67	0.391	0.025	0.014	–	–	–	73	0.860	611	5.28(r1)
68	0.396	0.027	0.011	–	–	–	74	0.854	629	5.46(r1)

(continued)

Table 3 (continued)

<i>Grt</i>				<i>Opx</i>			<i>Crd</i>			
Spot	X_{Mg}	X_{Ca}	X_{Mn}	Spot	X_{Mg}	X_{Al}	Spot	X_{Mg}	$T, ^\circ C$	$P, \text{ kbar}$
69	0.391	0.028	0.013	–	–	–	75	0.855	621	5.36(r1)
63	0.379	0.017	0.012	–	–	–	65	0.852	614	5.22(r1)
64	0.367	0.017	0.011	–	–	–	65	0.852	601	5.02(r1)
66	0.395	0.021	0.013	–	–	–	73	0.860	615	5.34(r1)
118	0.355	0.020	0.009	–	–	–	119	0.859	574	4.72(r1)

* $X_{Mg} = Mg/(Mg + Fe)$, $X_{Ca} = Ca/(Ca + Mg + Fe)$, $X_{Mn} = Mn/(Mn + Ca + Mg + Fe)$, $X_{Al} = Al/(Al + 2Mg + 2Fe)$; **temperatures were calculated using the *Grt-Crd* thermometer (reaction r2 of Table A2-1) while pressures were calculated using reactions r1 and r5 from Table A2-1

cordierite as a result of reaction $Crd \Rightarrow Grt + Sil + Qtz$ (Fig. 4c, d); atollitic garnet with quartz inclusions resulted from reaction $Crd + Opx \Rightarrow Grt + Qtz$; euhedral or atollitic garnet with quartz inclusions and/or sillimanite after plagioclase resulted from reaction $Pl \Rightarrow Grt + Qtz + Sil$.

III. Reaction textures resulting from the hydration of garnet, orthopyroxene and cordierite.

As a rule, reaction textures of type I are common for metapelites from the studied terrains, and reaction textures of type II are more characteristic of the rocks from the marginal zones. In some samples the isobaric cooling reaction textures (type II) are superimposed on the decompression cooling reaction textures (type I). Very rarely (e.g., samples lg-33 and lg-34, Table 2) reaction textures of the first type are developed after textures of the second type. In contrast, reaction textures of type III are superimposed on all types of textures.

Some of the samples studied from the CZ of the Limpopo HGT (BY27, BY30, Table 2, Fig. 1) do not contain distinct reaction textures of the first or second types. However, their *P-T* paths are recorded by zoning of coexisting minerals (the $Grt + Crd + Opx + Pl + Qtz$ and $Grt + Crd + Sil + Pl + Qtz$ assemblages).

Reaction textures and mineral zoning reflecting decompression cooling

The *Crd-Opx* coronas developed around garnet in contact with quartz. Samples LW7 and KL1098 (Table 2) demonstrate the best examples of reaction texture that formed due to the following reaction:



In spite of differences in thickness, the *Crd-Opx* coronitic textures from both complexes show regular mineral and chemical zoning:

- cores of the coronas are large relict garnet porphyroblasts whose N_{Mg} decrease by 8–12 from the core to the rim (Fig. 4a, b);
- the *Crd-Opx* symplectite is preserved at the contact with garnet, while the grain size of the symplectite minerals increases towards the corona margins;

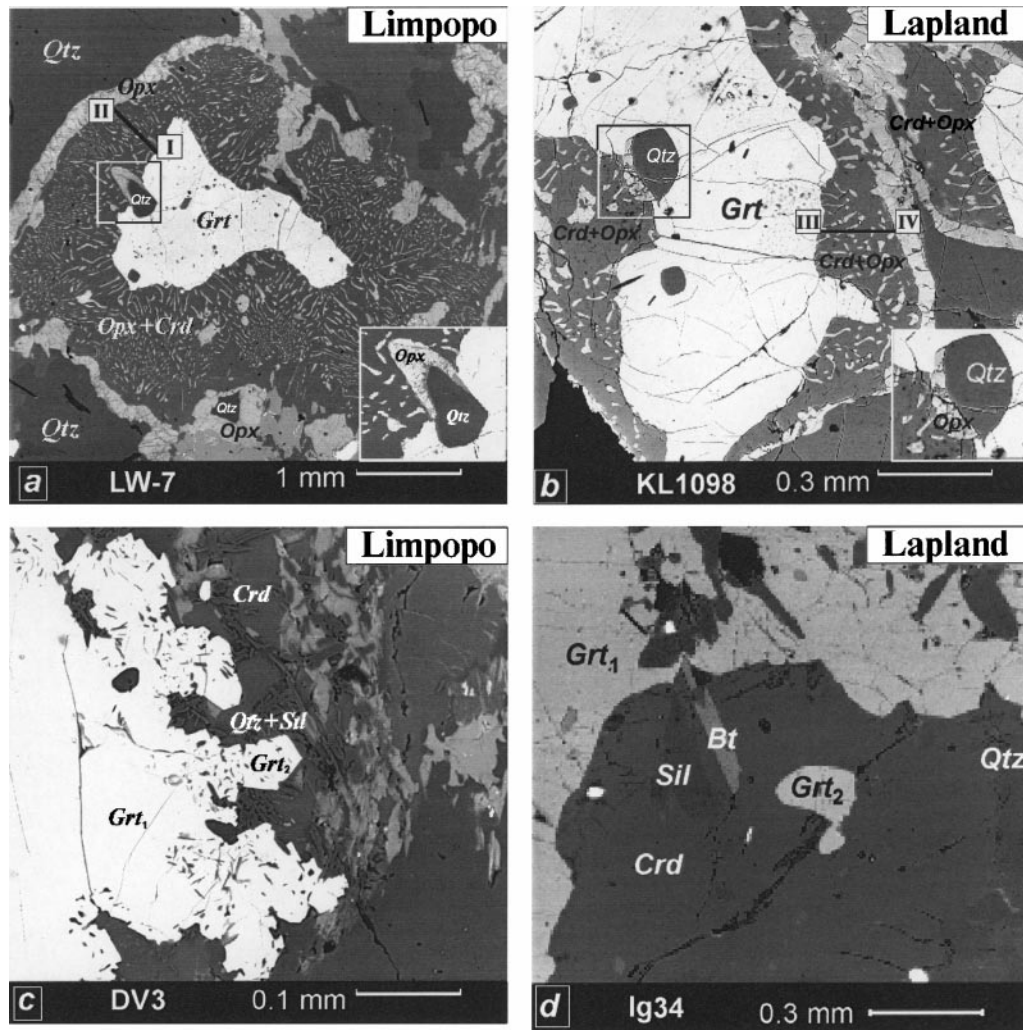


Fig. 4. Reaction textures preserved in metapelites from the SMZ of the Limpopo and Lapland HGTs. **a** and **b** *Opx* + *Crd* symplectites and *Opx* coronas formed after reaction (1), $Grt + Qtz \Rightarrow Opx + Crd$. **c** and **d** the assemblage *Grt* + *Sil* + *Qtz* newly formed after cordierite through reaction (5), $Crd \Rightarrow Grt + Sil + Qtz$. Reflected electrons, CamScan electron microscope. Chemical profiles (see Fig. 5a and b) are shown by solid lines

- in contact with quartz, the symplectites are mantled with monomineralic orthopyroxene coronas;
- the monomineralic orthopyroxene coronas developed also around quartz inclusions in garnet that had formed in the course of reaction (1);
- cordierite or pure sodic plagioclase occur between the symplectites and external orthopyroxene zones.

Figures 5a and 5b show a consistent change in the chemical composition of the corona in terms of N_{Mg}^{Opx} , N_{Mg}^{Crd} and N_{Al}^{Opx} . Both the N_{Mn} and the N_{Ca} of the relict

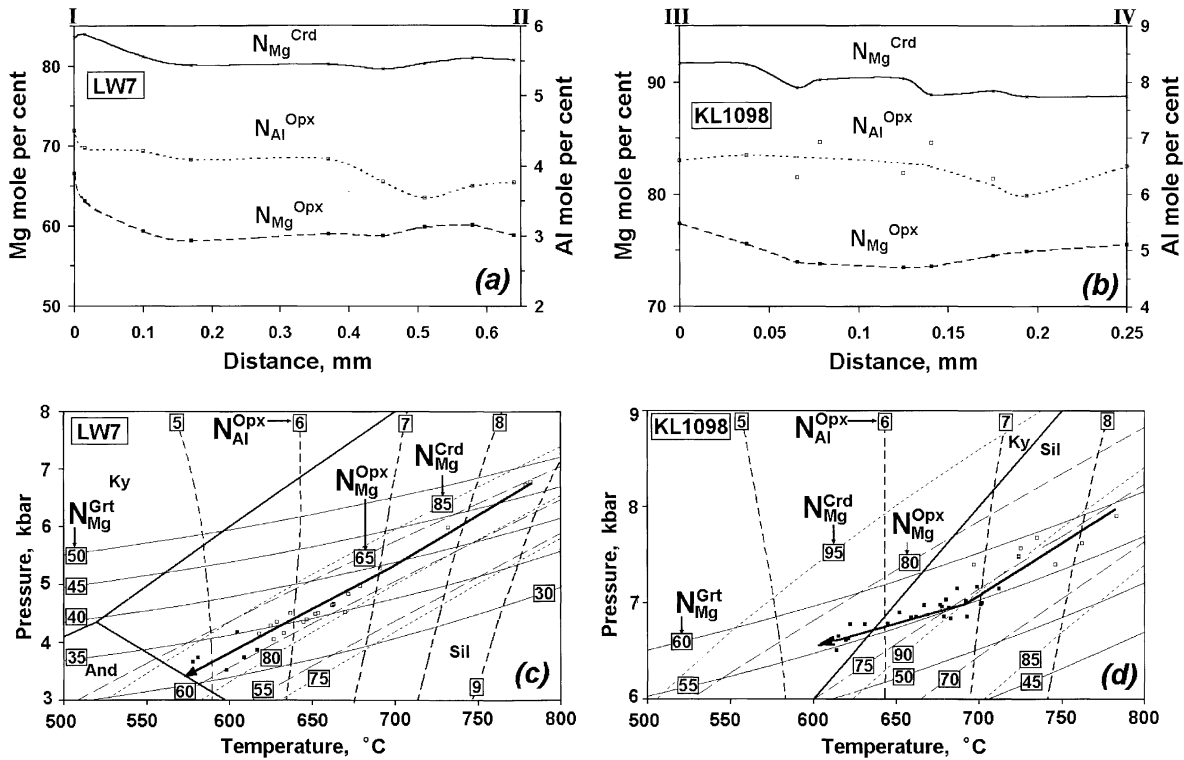
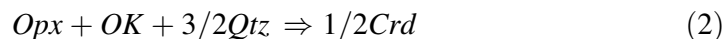


Fig. 5. Compositional and thermodynamic evolution of metapelites from the SMZ of the Limpopo (LW7, diagrams **a** and **c**) and Lapland (KL1098, diagrams **b** and **d**) HGTs. **a** and **b** Changes in the composition of contacting *Crd* and *Opx* in the cordierite-orthopyroxene symplectite formed between *Grt* and *Qtz*; the left portions of the profiles (solid lines in Fig. 4) correspond to the contact between the *Opx* corona and relict *Grt*, while the right portion corresponds to the contact between the corona and the outer *Opx* mantle. **c** and **d** Decompression cooling *P-T* paths (arrows) for metapelites summarizing the results of thermobarometric calculations (rectangles) based on reaction $Grt + Qtz \Rightarrow Opx + Crd$. Solid rectangles define *P-T* parameters calculated for rims of contacting minerals, while open rectangles reflect those for cores

garnet differ slightly between the core and the rim. Reaction (r5) in Table A2-1 is considered responsible for the formation of the *Crd-Opx* coronitic textures. As this reaction shows relatively small ΔH^0 at large ΔV^0 (see Table A2-1 in Appendix 2), and proceeds to the right with decreasing pressure, the corona texture must have been formed at the retrograde stage of metamorphism (Harley, 1989; Perchuk, 1989; Perchuk et al., 1996) and the *P-T* path obtained with the *Grt-Crd-Opx-Qtz* geothermobarometer (Aranovich and Podlesskii, 1989) reflects regular changes in N_{Mg}^{Grt} and N_{Al}^{Opx} and insignificant changes in N_{Mg} of both orthopyroxene and cordierite in the reaction texture (Fig. 5c and d). The N_{Al}^{Opx} decreases in the cordierite-bearing assemblages may have resulted from the reaction



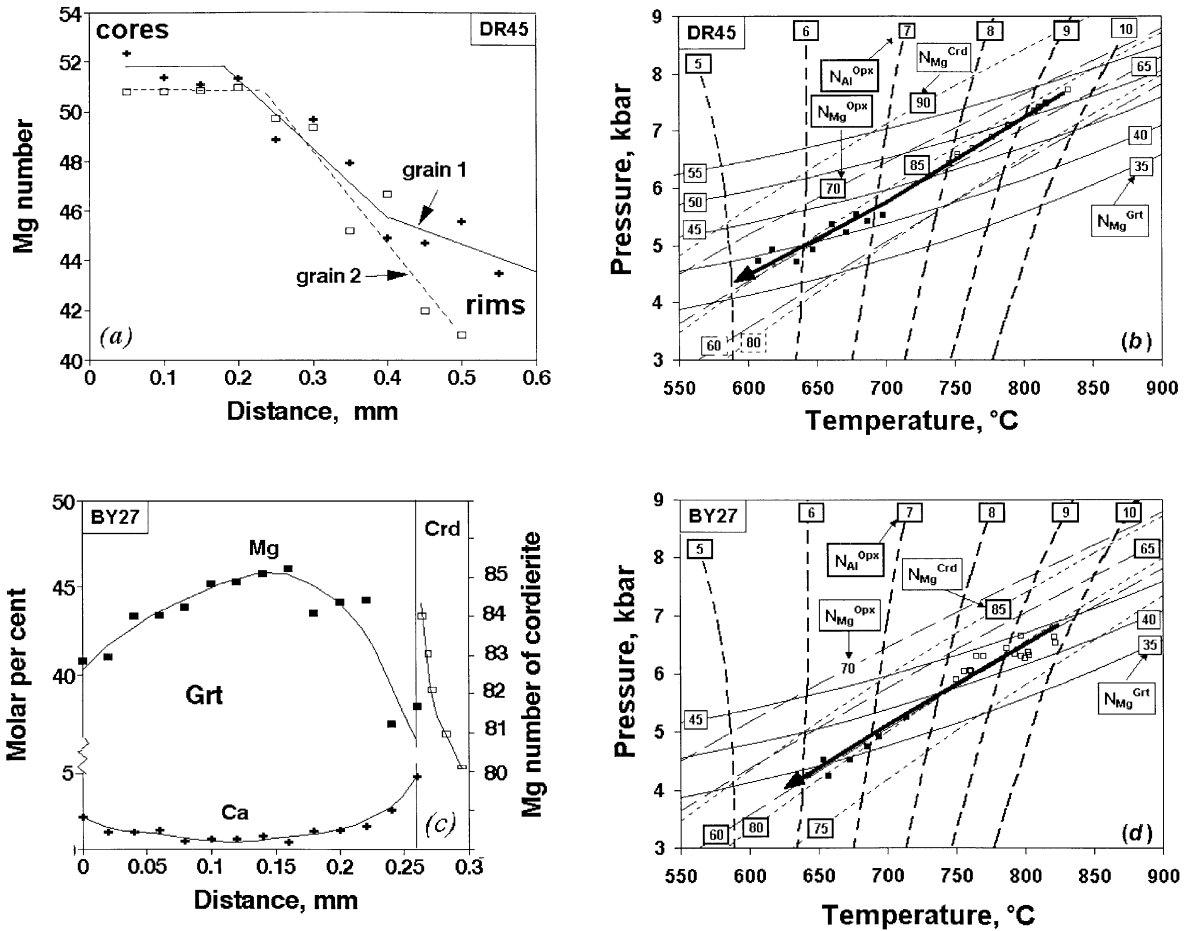
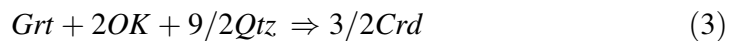


Fig. 6. Comparison of the compositional and thermodynamic evolution for two metapelites from different zones of the Limpopo HGT. **a** microprobe profiles for two garnet porphyroblasts of sample DR45. **b** P - T path for sample DR45; solid rectangles define P - T parameters calculated for rims of contacting minerals, while open rectangles reflect those for cores (see Appendix 2). **c** Microprobe profile across a garnet porphyroblast in contact with cordierite in sample BY27. **d** P - T path for sample BY27 calculated using data for reactions r2 and r5 (Table A2-1); solid rectangles define P - T parameters calculated for rims of contacting minerals, while open rectangles reflect those for cores

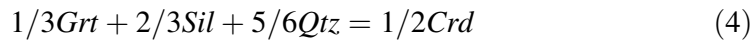
The Crd - Opx corona around garnet in contact with the matrix orthopyroxene is identical to the corona described above. For example, the corona in metapelite DV81 (Table 2) from the Limpopo HGT is composed of cordierite with coarse inclusions of relic orthopyroxene of variable morphology and size. The aluminum content of the relic orthopyroxene in the corona is appreciably lower compared with that of the primary matrix orthopyroxene. The decrease in the aluminum content of orthopyroxene corresponds to the reaction



accompanied by reactions (1) and (2), which suggests that the textures must have formed due to decomposition of garnet in the assemblage $Grt + Crd + Opx + Pl + Qtz$. Garnet in sample DR45 shows systematic chemical zoning (Fig. 6a). The P - T path in Fig. 6b shows a conjugate change in the composition of the contacting minerals and indicates a decompression-cooling metamorphic regime for the HGT. The upper portion of the P - T path corresponds to the constant composition of the garnet core (Fig. 6a) and reflects a metamorphic peak of about 7.8 kbar and 835 °C.

Sample BY27 (Table 2) from the CZ of the Limpopo HGT does not contain reaction textures, and the compositional evolution is recorded only in chemical zoning of coexisting garnet, cordierite, and orthopyroxene. Cores of the large garnet grains in this sample have $N_{Mg}^{Grt} = 46$, while N_{Mg}^{Grt} of the rims varies between 41 and 37 (Fig. 6c). The cores contain numerous inclusions of quartz and biotite, while the outer zones are inclusion-free. Cordierite in the matrix shows $N_{Mg} = 80$ –82 that systematically increases towards the contact with garnet (Fig. 6c). Cordierite is often replaced with the ragged secondary biotite or with aggregates of chlorite and muscovite. Orthopyroxene forms crystals up to 5 mm large with $N_{Mg}^{Opx} = 67$ –64, while N_{Al}^{Opx} decreases from 7 to 5 towards the rims. The P - T path of sample BY27 taken from the CZ also reflects a common decompression cooling history (Fig. 6d) similar to that of samples DR45, LW7 and DV81 from the SMZ of the Limpopo belt.

The divariant equilibrium



occurs in metapelites from the both granulitic complexes. Garnet porphyroblasts from metapelites Ig-33 and Ig-34 (Table 2) of the Lapland HGT have complex shapes. Their cores ($N_{Mg}^{Grt} = 36$) are filled with oriented inclusions of biotite, quartz, and sillimanite, with the latter presented both by the large inclusions and the fibrolite needles. Cordierite with $N_{Mg}^{Crd} = 76$ –78 forms large grains of different shape around garnet and contains separate inclusions of sillimanite, quartz, and garnet. In places, the Crd - Qtz intergrowths and coronas occur around the garnet porphyroblasts (Perchuk et al., 1999a).

The iron rich metapelite BY30 (Table 2) from the CZ of the Limpopo HGT also does not contain any distinct reaction textures. The P - T history of this sample is recorded by the garnet-cordierite equilibrium (4). The cores of the garnet porphyroblasts with $N_{Mg}^{Grt} = 29$ –30 and $N_{Ca}^{Grt} = 2$ (Fig. 7a) contain oriented inclusions of quartz, spinel, ilmenite, rutile, and rare sillimanite. The preferred orientation of these inclusions suggests growth of the garnet at peak metamorphic and deformational conditions. The cores are overgrown by a second generation of garnet containing sillimanite inclusions. In places, the inclusions can often be traced into the matrix of the rock. N_{Mg}^{Grt} decreases to 20 in the rim, while N_{Ca}^{Grt} changes from 2 to 3.5. Some of the garnet grains are cracked, and these cracks are filled with cordierite. The cordierite remote from the garnet has the Mg number of 69. In direct contact with the garnet, N_{Mg}^{Crd} increases up to 72 and reflects the Fe-Mg exchange (Fig. 7a). Sillimanite in the rock occurs as sheaf-like mantles around garnet in contact with cordierite and as clusters in the cores of cordierite. The observed simultaneous decrease in N_{Mg}^{Grt} and the increase in N_{Mg}^{Crd} towards the rims reflect cooling, while the cordierite growth in micro-cracks in the garnet indicates decrease in pressure due shift of reaction 4 to the right side (Fig. 7b).

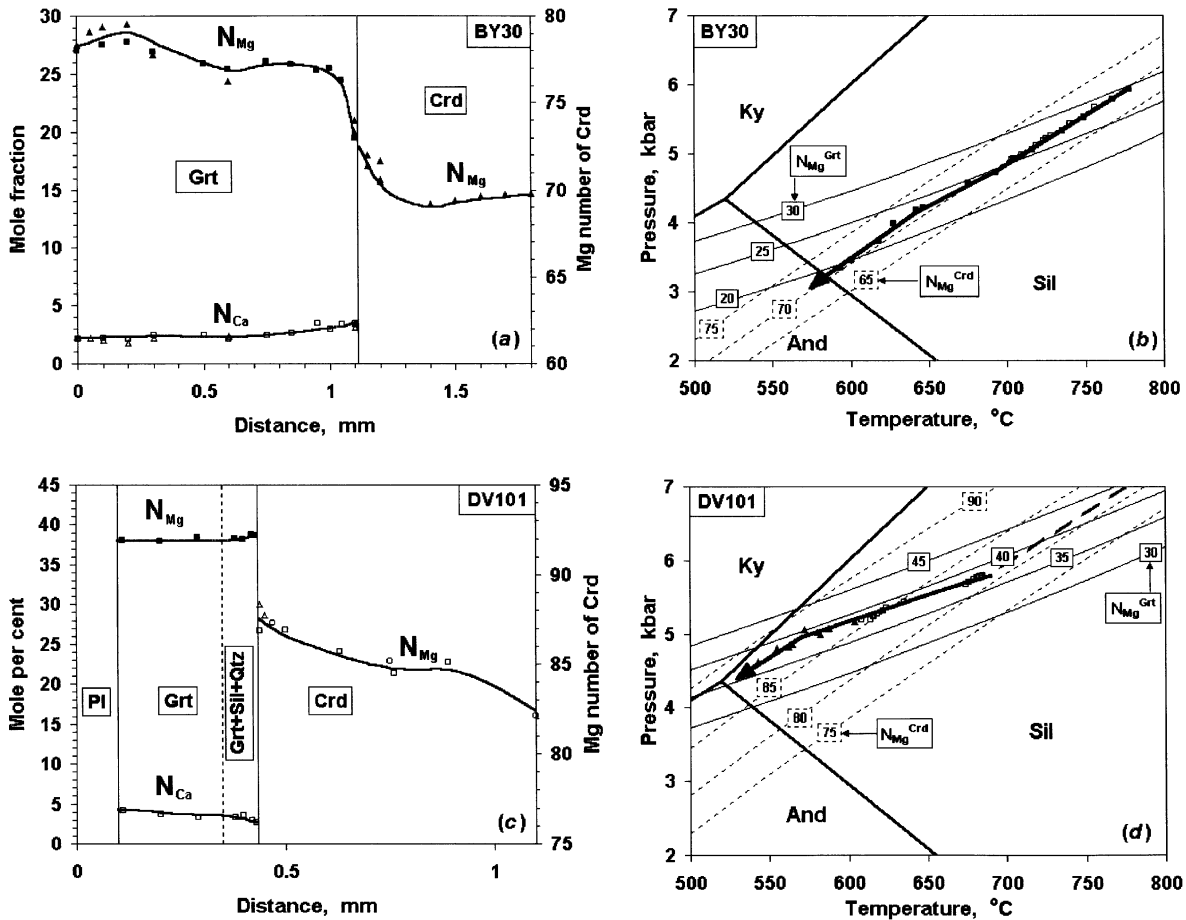
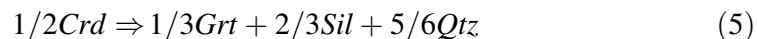


Fig. 7. Comparison of the compositional and thermodynamic evolution for two metapelites from different zones of the Limpopo HGT. **a** Microprobe profile across the contact of garnet and cordierite from metapelite BY30. **b** P - T path for Sample BY30 calculated using data for reactions r2 and r1 (Table A2-1); solid rectangles define P - T parameters calculated for rims of contacting minerals, while open rectangles reflect those for cores. **c** Microprobe profile across the contact of garnet and cordierite from metapelite DV101; **d** P - T path calculated for Sample DV101 using data for reactions r2 and r1 (Table A2-1); solid triangles define P - T parameters calculated for rims of contacting minerals, while open rectangles reflect those for cores. Early decompression cooling (thick dashed line) presumably corresponds to the replacement of early garnet by the *Opx-Crd* intergrowth

Reaction textures and mineral zoning reflecting isobaric cooling

The *Grt-Sil* reaction textures after cordierite

The delicate intergrowth of euhedral garnet and sillimanite which developed after cordierite was first described in metapelites from the Kanskiy HGT, Yenisey Range (Perchuk et al., 1989). This texture resulted from the reaction



Similar textures were observed in metapelites from both the SMZ of the Limpopo HGT (e.g., DV3, DV81, DV101, R8; Table 2) and the Lapland HGT (e.g., lg-33 and lg-34, Table 2) and are demonstrated in Fig. 4c, d. As a rule, the new generation of garnet filled with the sillimanite inclusions forms separate euhedral grains on earlier cordierite or occurs as overgrowth relics of earlier garnet in contact with cordierite.

In metapelite DV3 (Table 2, Fig. 4c), the different generations of garnet show different Mg-numbers: (1) large homogeneous crystals of garnet show $N_{\text{Mg}}^{\text{Grt}} = 30-32$ at $N_{\text{Ca}}^{\text{Grt}} = 3-3.5$, and (2) the newly-formed tiny euhedral garnet ($N_{\text{Mg}}^{\text{Grt}} = 36$) grains contain inclusions of sillimanite and quartz and replace the *Crd-Opx* corona at $N_{\text{Mg}}^{\text{Crd}} = 85-82$, $N_{\text{Mg}}^{\text{Opx}} = 62$ and $N_{\text{Al}}^{\text{Opx}} = 3$. Orthopyroxene is preserved as relics in cummingtonite formed as a result of an increase of $a_{\text{H}_2\text{O}}$ in the metamorphic fluid (*van Reenen*, 1986).

Both the forward (4) and reverse (5) reactions are observed in sample lg-34 (Table 2, Lapland HGT) in which garnet contains inclusions of sillimanite and quartz. Growth of cordierite over garnet with $N_{\text{Mg}}^{\text{Grt}} = 36$ (in the core) must have led to a decrease in $N_{\text{Mg}}^{\text{Grt}}$ to 30–31 (Fig. 8a). According to thermobarometric estimates at $X_{\text{H}_2\text{O}}^{\text{fl}} = 0.2$ (for details see Table A2-2 in Appendix 2), reaction (4) yields cooling (Fig. 8b) from 800 °C to 715 °C and decompression from 6.7 to 5.7 kbar. Reaction (4) must have been followed by the reverse reaction (5) that indicates near-isobaric cooling from 675 °C to 625 °C and from 5.3 to 5.0 kbar (Fig. 8b). The newly-formed *Grt-Sil* assemblage replaces cordierite rims (Fig. 4d). Similar to DV3, $N_{\text{Mg}}^{\text{Grt}}$ in lg-34 increases to 33 in the outer garnet-sillimanite zone, whereas $N_{\text{Mg}}^{\text{Crd}}$ increases towards the garnet contact. In some parts of the sample, $N_{\text{Mg}}^{\text{Grt}}$ decreases from 31 in the cores to 20 in the rims (Fig. 12). At $N_{\text{Mg}}^{\text{Grt}} = 26$ in the margin, garnet is replaced by late cordierite ($N_{\text{Mg}} = 77-79$) and biotite ($N_{\text{Mg}} = 60$). This replacement is recorded as the lower portion of the *P-T* path in Fig. 8b.

The *Grt-Qtz* reaction texture after the *Crd-Opx* symplectite

This texture reflects the reverse of reaction (1). In granulite DV101, the *Crd-Opx* symplectites, which are products of the primary *Grt-Qtz* breakdown, are surrounded by the newly-formed garnet with $N_{\text{Mg}}^{\text{Grt}} = 38-40$ (Fig. 7c). Some of the crystals accreted to form an atollitic aggregate. The delicate lace-like *Grt-Qtz-Sil* intergrowth formed at the contact of the garnet with the outer cordierite. On the inner side of the atollitic garnet, the *Grt-Qtz* intergrowth replaces plagioclase. The Mg number of cordierite increases from 82 to 87 towards the contact with garnet (Fig. 7c). In places, outside the atollitic texture, the *Grt-Sil* symplectite is recrystallized into a solid sillimanite mantle located between garnet and cordierite with $N_{\text{Mg}}^{\text{Crd}} = 89$. $N_{\text{Al}}^{\text{Opx}}$ in metapelite DV101 decreases towards the orthopyroxene contact with the atollitic garnet. Therefore, the metapelite DV101 history is recorded by the successive growth and decomposition of the different mineral assemblages along the *P-T* path. During the earliest stage of the metamorphic evolution, the *Crd-Opx* symplectites after the primary pyrope-rich garnet were formed during the decompression cooling from the peak metamorphic conditions to $T = 675$ °C and $P = 5.7$ kbar. The near-isobaric path shows the temperature decrease from 675 °C

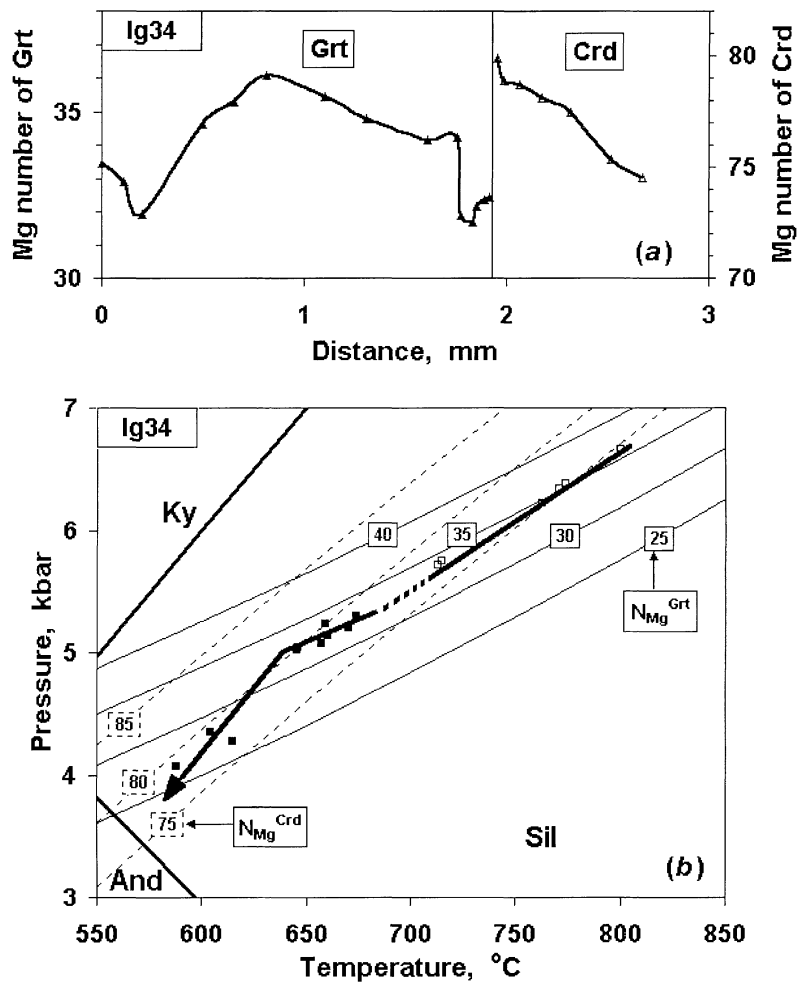


Fig. 8. Chemical zoning of coexisting garnet and cordierite (a) and P - T path (b) calculated using data for reactions r2 and r1 (Table A2-1) for sample Ig-34 from the Lapland HGT. Solid rectangles define P - T parameters calculated for rims of contacting minerals, while open rectangles reflect those for cores

to 575 °C, while pressure changes from 5.7 to 5.0 kbar. The atollitic garnet of $N_{Mg} = 38-40$ replaces orthopyroxene and cordierite after reaction



that proceeds simultaneously with reaction (5) and yields the Grt - Sil - Qtz symplectites.

The mineral chemistry and reaction textures in metapelite DR19 (Fig. 9a) are similar to those of sample DV101 (Fig. 7c). Figure 9b reflects the P - T path recorded in mineral assemblages of sample DR19 (detailed description of this sample and its P - T path is given in Appendix 2).

In metapelite R8 from the Limpopo HGT, the newly-formed Grt - Sil intergrowth occurs on the relic garnet rims in contact with the Crd - Opx

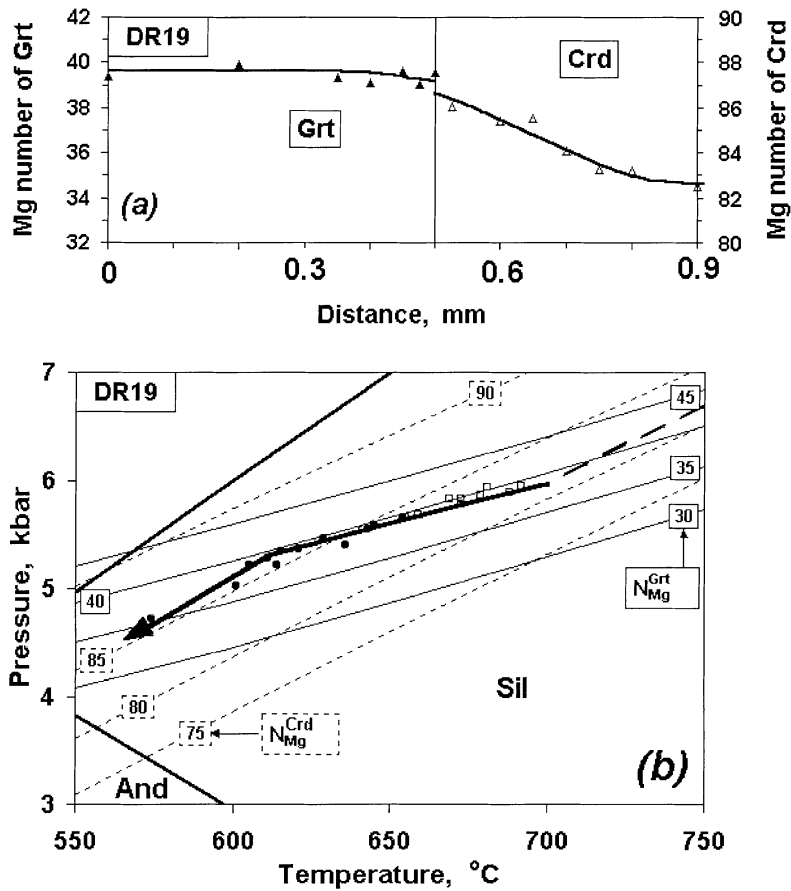


Fig. 9. Chemical zoning of coexisting garnet and cordierite (a) and P - T path (b) deduced for metapelite DR19 from the Limpopo HGT; solid circles define P - T parameters calculated for rims of contacting minerals, while open rectangles reflect those for cores (see Appendix 2). Early decompression cooling (thick dashed line) presumably corresponds to the replacement of early garnet by the *Opx-Crd* symplectite

symplectite. $N_{\text{Mg}}^{\text{Grt}}$ in the *Grt-Sil* symplectite is similar to the porphyroblast core. Presumably, this garnet was formed due to reverse reactions (5) and (6) at the near-isobaric (6.3–5.8 kbar) cooling (700–600 °C) stage of the P - T history (Fig. 14). As in sample DV3, the latest assemblage in granulite R8 is *Ged-Ky*, which suggests intensive hydration of the *Crd-Opx* symplectite to form biotite and cummingtonite with decreasing temperature (the reaction texture of type III).

Like sample R8, metapelite DV81 contains the *Grt-Qtz* and *Grt-Qtz-Sil* intergrowths on the rims of irregular garnet porphyroblasts in contact with the *Crd-Opx* symplectite. At constant $N_{\text{Mg}}^{\text{Grt}} = 43-45$, N_{Ca} changes from 7 in the core to 3 in the rim (Fig. 10a). At the contact with this garnet, $N_{\text{Mg}}^{\text{Crd}}$ varies within the range 85–88. The *Crd-Opx* symplectite resulted probably from the Mg-rich garnet breakdown at the early decompression-cooling stage of the sample P - T history (dashed line in Fig. 10b). This is supported by the high Ca content of the garnet core which is identical to that of the peak garnet from sample DR45 (Table 3).

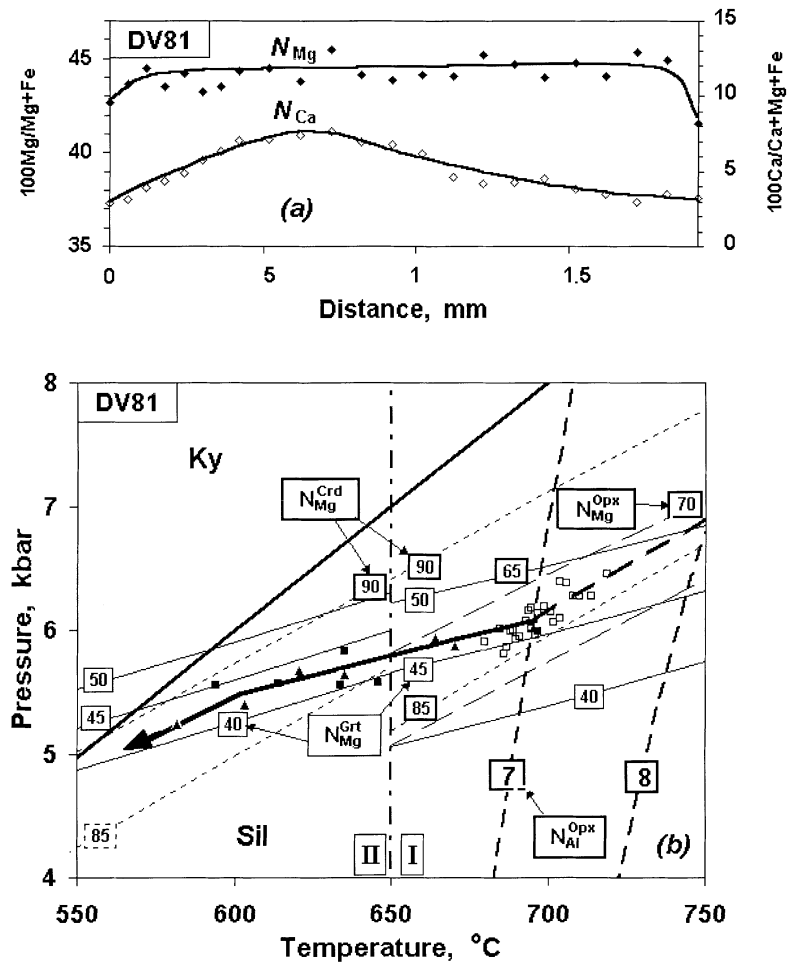


Fig. 10. Chemical zoning of irregular garnet porphyroblast located within *Opx-Crd* reaction texture (a) and *P-T* path (b) recorded in Sample DV81 from the Limpopo HGT. Symbols in the diagram refers to individual *P-T* calculations based on reactions r2 and r5 (rectangles), and r2 and r1 (triangles) from Table A2-1. The isopleths for the assemblage *Crd + Opx + Qtz + Grt* are shown in field I, while those for the assemblage *Crd + Grt + Sil + Qtz* are shown in the field II. Solid symbols define *P-T* parameters calculated for rims of contacting minerals, while open symbols reflect those for cores. Early decompression cooling (thick dashed line) presumably corresponds to the replacement of early garnet by *Opx-Crd* intergrowth

Formation of the *Grt-Qtz* and *Grt-Qtz-Sil* intergrowths on the garnet rims suggests simultaneous proceeding of reverse reactions (5) and (6) at the near-isobaric cooling stage of the *P-T* evolution (Fig. 10b). Replacement of the *Opx + Crd + Pl* assemblage by the atollitic garnet of $N_{Mg} = 43-44$ in contact with quartz was also observed in metapelite DV81 (Table 2).

Reaction textures resulting from the growth of the assemblage
Grt + Qtz ± *Sil* after *Pl*

Plagioclase coronas around garnet are very common in the HGT rocks (e.g. *Perchuk et al.*, 1985, 1989). Normally, these textures reflect decompressional cooling (*Harley*, 1989). On the other hand, a systematic increase in N_{Ca}^{Grt} of the newly-formed garnet (e.g., Fig. 11a, b) during the sub-isobaric cooling is controlled by the following reaction:



Corresponding reaction textures were found in many of the studied samples (e.g., DV101, R8, DV3). For example, a microprobe profile across the garnet grain from granulite DV3 shows a sharp increase in N_{Ca}^{Grt} at the contact with plagioclase. This increase is linked to the presence of the tiny euhedral garnet crystals that are separated from the larger grain accompanied by delicate quartz inclusions, while the sillimanite needles occur at the contact with plagioclase.

In metapelite DV81, the atollitic garnet of constant composition ($N_{Ca} = 2.9-3.7$, $N_{Mg} = 43-44$) grows in assemblage with orthopyroxene, cordierite, and plagioclase. At the contact with plagioclase, the delicate *Grt-Qtz* intergrowth occurs (Fig. 11b). The euhedral garnet inclusions (Fig. 11b) in plagioclase show $N_{Mg}^{Grt} = 43$, and $N_{Ca}^{Grt} = 3.3$. N_{Al}^{Opx} decreases towards the contact with the atollitic garnet inside the “ring”, while N_{Mg}^{Opx} increases. Such relationships must have resulted from the following reaction



that governs the garnet growth upon near-isobaric cooling (Fig. 10b).

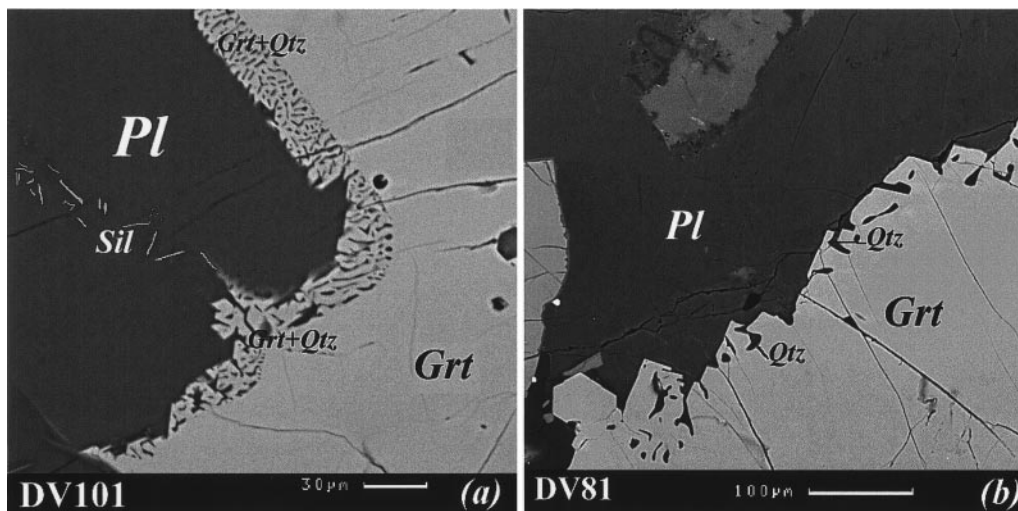
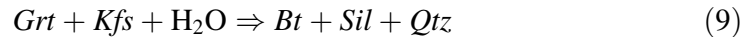


Fig. 11. The *Grt + Qtz* intergrowth at the contact of garnet with plagioclase in two metapelites from the SMZ of the Limpopo HGT. Reflected electrons, CamScan scanning electron microscope

Reaction textures and mineral zoning resulting from hydration

Biotite in samples lg-33 and lg-34 from the Lapland HGT is present as at least two generations, i.e. as separate grains and as intergrowths with quartz and sillimanite. The *Bt + Sil + Qtz* symplectites (Fig. 12) must have developed between garnet and K-feldspar as a result of the following reaction



This reaction allows to calculate a water activity of 0.2 ± 0.02 using thermodynamic data from reaction (r7) of Table A2-1 in Appendix 2.

Near the boundary of the SMZ, the Limpopo metapelites (samples DV3 and R8; in Table 2) often contain secondary orthoamphibole and the late *Bt + Ky* paragenesis, that replaces orthopyroxene and cordierite (*van Reenen*, 1986). Metapelite BY27 from the CZ of the Limpopo HGT (Table 2) is characterized by numerous hydration textures. In places, orthopyroxene, cordierite, and K-feldspar are replaced by the *Bt + Pl + Qtz* symplectite as a result of reaction r9 in Table A2-2 from Appendix 2. Using this reaction, the water activity was calculated within very narrow limits (0.18–0.21) that are similar to those obtained above from reaction (9).

Reaction textures in metabasites and the P-T conditions of their formation

Large volumes of metabasites occur in the NMZ of the Limpopo HGT (e.g., *Rollinson*, 1993; *van Reenen* et al., 1990, 1992; *van Reenen* and *Smit*, 1996) and eastern portion of the Lapland HGT (e.g., *Mints* et al., 1996; *Perchuk* et al., 1999a). In contrast to metapelites, these rocks were not thoroughly studied because they normally generate poor *P-T* information due to a lack of the reaction textures. This

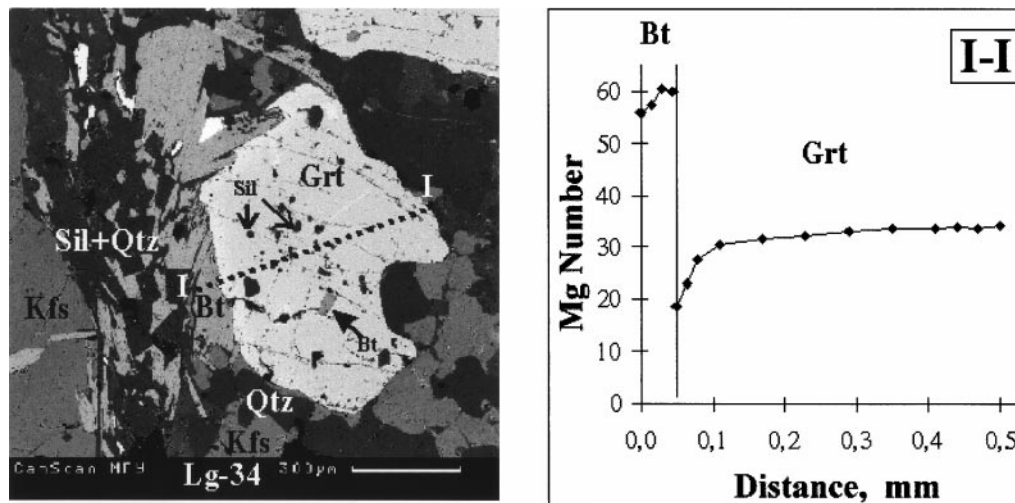


Fig. 12. The *Bt + Sil + Qtz* symplectite (electron microscope image) resulted from reaction (9) during the retrogression of sample lg34 and a micro-probe profile across the contact of biotite and garnet

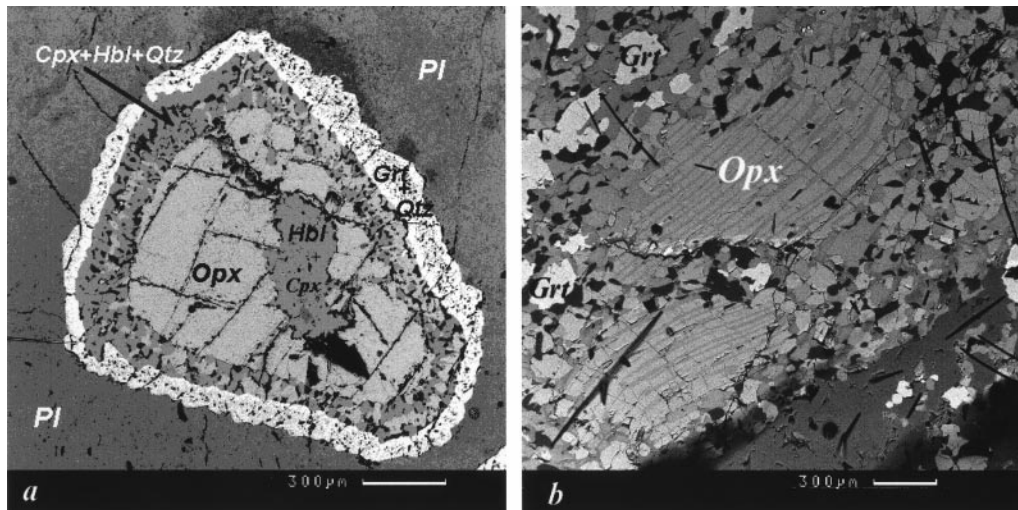


Fig. 13. Post-kinematic (a) and syn-kinematic (b) coronitic textures in gabbro-anorthosites from the Lapland HGT (in the area of the Kandalaksha Gulf, the White Sea). Electron microscope images (Larikova, 1996)

also applies to metabasites from the Lapland HGT presented by the *Bt-Opx-Pl-Grt* gneisses intercalated with the *Cpx-Grt* rocks and the *Grt-Hbl-Cpx* gneisses juxtaposed onto amphibolites of the Tanaelv belt (see Fig. 2).

In the Lapland HGT, the volume of basic granulites decreases from the east to the west. In the east, in the Salnie Tundry area, they dominate in the cross-section, while in Finland they are subordinate to the khondalite rock series (e.g., Eskola, 1952; Barbey and Raith, 1990). The characteristics, classification, *P-T* parameters of formation and origin of the Lapland metabasites were described in many publications (e.g., Sharkov et al., 1994; Alekseev et al., 1998). Among the metabasites (meta-anorthosites, meta-gabbro, etc.) of the eastern portion of the Lapland complex there are many coronites whose relation to the Lapland granulite body is still unclear.

Figure 13a, b demonstrates two examples of post-kinematic and syn-kinematic coronas in gabbro-anorthosites. Mints et al. (1996) suggest that the rocks belong to the underlying suite of the Lapland body, while others (e.g., Kozlov et al., 1990) attribute them to the Tanaelv belt, because some of them are strongly deformed. On the other hand, Perchuk et al. (2000b, this volume, sample Ig-20 in Table 2) found relics of epidote and hornblende in pyroxenes from *Grt-Cpx* rocks of the Tanaelv belt, which clearly indicate prograde metamorphism. This, therefore, implies that the rocks belong to the wall rocks (Tanaelv belt) of the Lapland HGT.

The metamorphic conditions of the Lapland metabasites were discussed in a few studies (Raith and Raase, 1982; Barbey and Raith, 1990; Daly and Bogdanova, 1991; Kozlov et al., 1990; Fonarev et al., 1994; Mints et al., 1996; Perchuk et al., 2000b, this volume). However, there is no general agreement on the *P-T* estimates of the different stages of metamorphism. Daly and Bogdanova (1991) obtained the highest *P-T* parameters from the metamorphosed enderbite that cuts metapelites: 910 °C and 8.7 kbar. For felsic granulites from the central part of the Lapland HGT,

they report temperature and pressure of 790 °C and 7.3 kbar. *Hörmann et al.* (1980) and *Raith and Raase* (1982) also distinguished two stages of metamorphism: a syn-kinematic stage ($T = 850\text{ °C}$, $P = 8\text{ kbar}$, $X_{\text{CO}_2}^{\text{fl}} > 0.8$) and a post-kinematic retrograde stage ($T = 830\text{--}760\text{ °C}$, $P = 7.2\text{--}6.2$, $X_{\text{CO}_2}^{\text{fl}} = 0.9\text{--}0.6$). These estimates are in good agreement with the data for metapelites described above (Fig. 8). In contrast to all these data, *Fonarev et al.* (1994) defined four metamorphic stages in the retrograde evolution of the Lapland granulites: (1) $T = 860\text{--}925\text{ °C}$ and $P = 11.3\text{ kbar}$, (2) $T = 780\text{--}810\text{ °C}$ and $P = 8.6\text{--}10.5\text{ kbar}$, (3) $T = 675\text{--}720\text{ °C}$ and $P = 7.6\text{--}7.7\text{ kbar}$, (4) $T = 565\text{--}605\text{ °C}$ and $P = 3.9\text{ kbar}$.

Discussion

Any reliable thermo-tectonic model for the formation of granulites must incorporate the full diversity of P - T paths from different parts of a HGT. As regards the P - T paths, all the studied samples can be subdivided into two groups:

- rocks with P - T trajectories that include an isobaric-cooling portion (Fig. 14a);
- rocks characterized only by decompression-cooling (Fig. 14b).

Harley (1989) reviewed both groups of P - T paths and concluded that they reflect different geodynamic histories. However, Fig. 14a and b demonstrate that metapelites from the two HGT studied show both types of P - T paths. In case of the Limpopo complex, most samples that preserve evidence for the common decompression-cooling P - T paths were collected far away ($> 45\text{ km}$) from the boundary of the SMZ with the KVC (see Fig. 1). On the other hand, along with the decompression-cooling stage, many of the P - T paths from the samples collected close to the boundary with the KVC also include an isobaric-cooling portion. The samples that preserve isobaric-cooling P - T paths (garnet growth reaction textures), have in fact never been collected from central portions of the complex. In case of

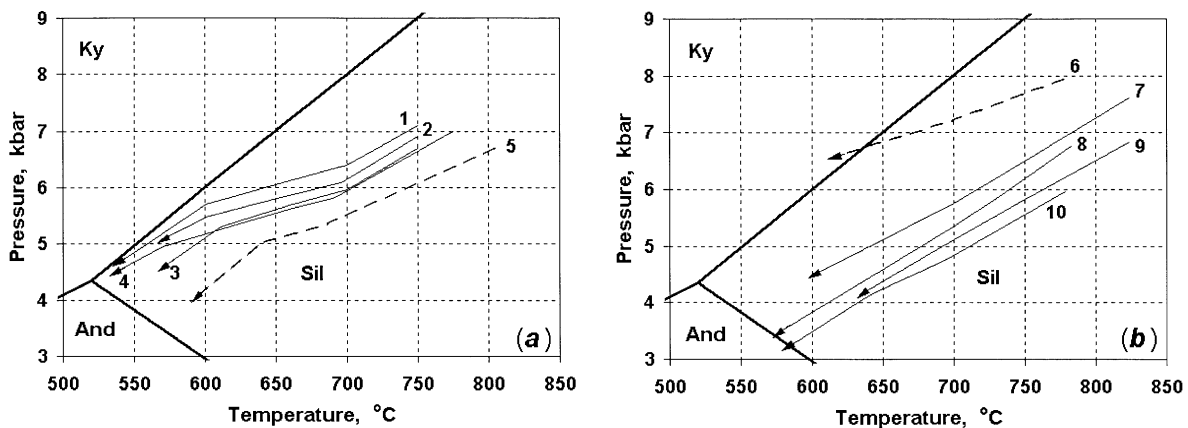


Fig. 14. P - T history of the Limpopo (solid lines) and Lapland (dashed lines) HGT. **a** Summarizes P - T paths for samples R8 (1), DV81 (2), DR19 (3), DV101 (4), Ig-34 (5) (Table 2). **b** Summarizes P - T paths for sample KL1098 (6), DR45 (7), LW7 (8), BY27 (9), BY30 (10) (Table 2)

the Lapland HGT, all samples with near-isobaric cooling portions of the P - T paths were collected at the northern boundary of the complex (Fig. 2b).

Perchuk et al. (1996) explained the existence of the two types of the P - T paths in the SMZ of the Limpopo HGT (Fig. 14a and b) by differences in the movement of different crustal blocks during their exhumation. The crustal blocks from central portions of the complexes were simply exhumed and adjusted to the normal thermal gradient of the crust during the exhumation (P - T path in Fig. 14b). The ascending blocks close to the boundary of the complexes were arrested at crustal levels of about 13–15 km, where they cooled rapidly (P - T path in Fig. 14a) because of the temperature gradient between the hot granulites and cooler underthrust greenstone plate (wall rocks for HGT). The near-isobaric parts of the retrograde P - T paths, therefore, may characterize the marginal zones of the Limpopo and Lapland HGT. On the other hand, the non-isobaric metamorphic zonation is well developed in sheared rocks of GSB adjacent to the HGT studied (e.g., *Roering et al.*, 1992b; *Przhjalgovsky and Terekhov*, 1995; *Perchuk et al.*, 1996; *Perchuk and Krotov*, 1998; see also *Perchuk et al.*, this volume). This also provides evidence for thermal and dynamic interaction between HGT and adjacent GSB during exhumation and cooling of granulites.

Conclusions

Comparative study of the Limpopo and Lapland complexes showed that

- both HGT are younger than their cratonic counterparts;
- the geometry of the high-grade bodies is similar to that of intrusive harpoliths;
- the HGT are bounded by the non-isobaric metamorphic zoning developed in the GSB;
- mineral zoning and reaction textures of HGT record both decompression cooling and near-isobaric cooling P - T paths (the latter characterizes the HGT margins); the two types of reaction textures and corresponding P - T paths reflect two different ways in which the rocks of the Limpopo and Lapland granulitic bodies were exhumed;
- the highest equilibrium pressures and temperatures for metapelites of the SMZ and CZ of the Limpopo HGT are 6.7–7.8 kbar and 820–830 °C; similar P - T conditions (6.7–7.9 kbar and 780–800 °C) were estimated for some metapelites of the Lapland HGT; the lowest P - T estimates for both HGT vary within 3.5–4.5 kbar and 530–600 °C.

Acknowledgments

Since 1995 this work was supported by FRD, Gencor and JCI grants to DDVR and RFBR grants # 96-05-64396, # 99-05-65605 and # 96-15-98470 to LLP. The final version of this paper benefited greatly from constructive reviews by *J.M. Barton*, *D. Harlov*, and *K.K. Podlesskii*.

References

- Alekseev NL, Lobach-Zhuchenko SB, Bogomolov ES, et al* (1998) Phase and isotopic (Nd) equilibria in coronites from the Tolstik and Tupaya Guba massifs, N-W Belomorie, the Baltic shield. *Petrology* 7(1): 3–23

- Aranovich LY, Podlesskii KK* (1989) Geothermobarometry of high-grade metapelites: simultaneously operating reactions. In: *Daly JS, Yardley BWD, Cliff BR* (eds) Evolution of metamorphic belts. Geol Soc London, Spec Publ 42: 41–65
- Barbey P, Raith M* (1990) The granulite belt of Lapland. In: *Vielzeuf D, Vidal Ph* (eds) Granulites and crustal evolution. Kluwer, Dordrecht, pp 111–132 (NATO ASI Series C)
- Barbey P, Convert J, Martin M, et al* (1980) Relationships between granite-gneiss terrains, greenstone belts and granulite belts in the Archean crust of Lapland (Fennoscandia). *Geol Rdsch* 69: 648–658
- Barbey P, Convert J, Moreau B, Capdevila R, Hameurt J* (1984) Petrogenesis and evolution of an Early Proterozoic collisional orogen: the Granulite Belt of Lapland and the Belomorides (Fennoscandia). *Bull Geol Soc Finland* 56: 161–188
- Barton JM Jr, van Reenen DD* (1992) The significance of Rb-Sr ages of biotite and phlogopite for the thermal history of the Central and SMZs of the Limpopo Belt of southern Africa and the adjacent portions of the KVC. *Precamb Res* 55(1–4): 17–31
- Barton JM Jr, du Toit MC, van Reenen DD, et al* (1983) Geochronological studies in the Southern Marginal Zone of the Limpopo mobile belt, southern Africa. *Geol Soc S Afr Spec Publ* 8: 55–64
- Bernard-Griffiths J, Peucat JJ, Postaire B, et al* (1984) Isotopic data (U-Pb, Rb-Sr, Pb-Pb and Sm-Nd) on mafic granulites from Finnish Lapland. *Precamb Res* 23: 225–348
- Bersthelsen A, Marker M* (1986) Tectonics of the Kola collision suture and adjacent Archean and Early Proterozoic terrains in the northeastern region of the Baltic shield. *Tectonophysics* 126: 31–55
- Berger M, Kramers JD, Naegler TF* (1995) Geochemistry and geochronology of charnoenderbites in the NMZ of the Limpopo Belt, southern Africa, and genetic models. *Schweiz Mineral Petrogr Mitt* 75: 17–42
- Bogdanova MN, Efimov MM* (1997) Belomorian-Lapland early Precambrian high-grade mobile belt. *EUG 9 [Abstr Suppl 1] to Terra Nova* 9: 363
- Bibikova EV, Melnikov VF, Avokian KKh* (1993) The Lapland granulites: petrology, geochemistry and isotopic age. *Petrology* 1: 215–234
- Bohlender F, van Reenen DD, Barton JM Jr* (1992) Evidence for the presence of igneous and metamorphic charnockites in the Southern Marginal Zone of the Limpopo Belt. *Precamb Res* 55: 429–449
- Daly JS, Bogdanova S* (1991) Timing of the metamorphism in the Lapland granulite belt, Finland. *Research of Terrae, ser A5*, 5: 11
- de Wit MJ, Roering C, Hart RJ, Armstrong RA, et al* (1992) Formation of an Archean continent. *Nature* 357: 553–562
- Eskola P* (1952) On the granulites of Lapland. *Am J Sci (Bowen Volume)* 1: 133–171
- Frisch T, Jackson GD, Glebovitskiy VA, et al* (1995) The U-Pb geochronology of the Kolvitsa gabbro-anorthosite complex, southern part of the Kola Peninsula. *Petrology* 3: 248–254
- Fonarev VI, Grafchikov AA, Konilov AN* (1994) Experimental investigations of equilibria involving mineral solid solutions. In: *Zharikov VA, Fedkin VV* (eds) Experimental problems in geology. Nauka Press, Moscow, pp 323–355 (in Russian)
- Gaal G, Berthelsten A, Gorbachev R, et al* (1989) Structure and composition of the Precambrian crust along the POLAR profile in the northern Baltic Shield. *Tectonophysics* 162: 1–25
- Gary M, McAfee R, Wolf CL* (1972) Glossary in geology. Am Geol Inst, Washington DC, 637 p

- Gerya TV* (1991) The method of physicochemical modeling of metamorphic reactions by using mass-balance condition. *Contrib Physicochem Petrol* 16: 112–127 (in Russian)
- Gerya TV, Perchuk LL* (1990) GEOPATH – a thermodynamic database for geothermobarometry and related calculations with the IBM PC computer. Program and Abstract, Calg Univ Press, Calgary, Canada, pp 59–61
- Gerya TV, Perchuk LL, Triboulet C, Audren C, Sesíko AI* (1997) Petrology of the Tumanshet metamorphic complex, eastern Sayan, Siberia. *Petrology* 5: 503–533
- Glebovitskii VA, Miller Yu V, Drugova GM, et al* (1996) Structure and metamorphism of the Belomorian-Lapland collision Zone. *Geotectonics* 1: 63–75
- Harley SL* (1989) The origin of granulites: a metamorphic perspective. *Geol Mag* 126: 215–231
- Harris NBW, Holland TJB* (1984) The significance of cordierite-hypersthene assemblages from the Beitbridge region of the Central Limpopo Belt; evidence for rapid decompression in the Archean. *Am Mineral* 69: 1036–1049
- Hofmann A, Kröner A, Brandl G* (1998) Field relationships of mid- to late Archean high-grade gneisses of igneous and sedimentary parentage in the Sand River, Central Zone of the Limpopo Belt, South Africa. *S Afr J Geol* 101: 185–200
- Holzer L, Kramers JD, Blenkinsop TG* (1997) Granulite facies metamorphism in the Limpopo Central zone (southern Africa): evidence for a Proterozoic continental collision between the Kaapvaal and Zimbabwe cratons. *EUG 9 [Abstr Suppl 1] to Terra Nova* 9: 365
- Holzer L, Frey R, Barton Jr JM, Kramers JD* (1998) Unraveling the record of successive high-grade events in the Central Zone of the Limpopo belt using Pb single phase dating of metamorphic minerals. *Precamb Res* 87: 87–115
- Hörmann PK, Raith M, Raase P, et al* (1980) The granulite complex of Finnish Lapland: petrology and metamorphic conditions in the Ivalojoiki-Inarijarvi area. *Geol Surv Finl Bull* 308: 1–95
- Hisada K, Miyano T* (1996) Petrology and microthermometry of aluminous rocks in the Botswanan Limpopo Central Zone: evidence for isothermal decompression and isobaric cooling. *J Metam Geol* 14(2): 183–197
- Jackson JA* (ed) (1997) Glossary of geology. Am Geol Inst, Virginia, 769 p
- Jaekel P, Kröner A, Kamo SL, Brandl G, Wendt JI* (1997) Late Archean to early Proterozoic granitoid magmatism and high-grade metamorphism in the Limpopo belt, South Africa. *J Geol Soc Lond* 154: 25–44
- Kamber BS, Biino GG* (1995) The evolution of high T-low P granulites in the Northern Marginal Zone sensu stricto, Limpopo Belt, Zimbabwe: the case for petrography. *Schweiz Mineral Petrogr Mitt* 75: 427–454
- Kozlov NE, Ivanov AA, Nerovich LI* (1990) The Lapland granulite belt (primary origin and evolution). *Rus Acad Sci, Kola Sci Center, Apatity*, 170 p (in Russian)
- Kreissig K, Holzer L* (1997) The Kaapvaal craton – SMZ (Limpopo belt) connection; implications from geochronological data, Pb isotopes and REE Patterns. *EUG 9 [Abstr Suppl 1] to Terra Nova* 9: 364–365
- Kröner A, Jaekel P, Hofmann A, Nemchin AA, Brandl G* (1998) Field relationships and age of supracrustal Beit Bridge Complex and associated granitoid gneisses in the Central Zone of the Limpopo Belt, South Africa. *S Afr J Geol* 101: 201–213
- Krill AG* (1985) Svecofokarelian thrusting with thermal inversion in the Karasjok-Levajok area of the northern Baltic Shield. *Nor Geol Unders* 403: 89–101
- Larikova TL* (1996) Comparable petrology of coronites from southern and northern shores of the Kandalaksha gulf, White Sea. Thesis, Moscow State University, 72 p (in Russian)

- Latyshev LN* (1971) Stratigraphy of supracrustal rocks from the Korva tundra. In: Stratigraphic division and correlation of the Precambrian of the N.-E. portion of the Baltic shield. Nauka Press, Leningrad, pp 61–65 (in Russian)
- Marker M* (1988) Early Proterozoic thrusting of the Lapland granulite belt and its geotectonic evolution, northern Baltic Shield. *Geol Foren Stockh Forh* 110: 405–410
- Marker M* (1990) Tectonic interpretation and new crustal modeling along the POLAR Profile, Northern Baltic Shield. In: *Freeman R, Mueller S* (eds) Data compilations and synoptic interpretation. 6th Workshop on the European geotraverse project. Proc Europ Sci Found, Strasbourg, pp 9–22
- Marker M* (1991) Metamorphism, deformations and structure of the crust. In: *Tuisku P, Laajoki K* (eds) Excursion guide to Lapland. University of Oulu, Finland, pp 38–66
- McCourt S, van Reenen DD* (1992) Structural geology and tectonic setting of the Sutherland Greenstone Belt, Kaapvaal Craton, South Africa. *Precamb Res*: 93–110
- Merilainen K* (1976) The granulite complex and adjacent rocks in Lapland, Northern Finland. *Geol Surv Finl Bull* 281: 1–129
- Mikkola F* (1937) Pre-Quaternary rocks, sheets C7 and D7, Sodankytä, Tuntajoki. General Geological Map of Finland 1:400 000. Geol Toimikunta, Helsinki
- Mikkola E* (1941) General geological map of Finland. Sheets B7, C7, D7, Muonio, Sodankytä, Tuntajoki. Explanation to the map of rocks, Suomen. Geol Toimikunta, Helsinki, 286 p
- Mints MV, Glaznev VN, Konilov AN, et al* (1996) The Early Precambrian of the North-Eastern Baltic shield: paleodynamics, crustal structure, and evolution. Moscow Scientific World Press, Moscow, 277 p (in Russian, with extended abstracts of all chapters in English)
- Mitrofanov FP, Balagansiy VV, Balashov YuA, et al* (1993) U-Pb age of gabbro-anorthosites from the Kola Peninsula. *Dokl Russ Akad Nauk* 331(1): 95–98
- Miyano T, Ogata H, van Reenen DD, et al* (1990) Peak metamorphic conditions of sapphirine-bearing rocks in the Rhenosterkoppies Greenstone Belt, northern Kaapvaal Craton, South Africa. In: *Glover JC, Ho SE* (eds) The Archaean: terranes, processes and metallogeny 22: 73–87
- Mkweli S, Blenkinsop TG* (1995) Metabasite amphibole compositional variations across the Umlali Thrust Zone of the Limpopo Belt, Zimbabwe: implications on the tectonics. Centennial Geocongress, Extended Abstracts II. Geol Soc S Afr, Johannesburg, pp 189–190
- Percival JA, Roering C, van Reenen DD, Smit CA* (1997) Tectonic evolution of associated greenstone belts and high-grade terranes. In: *de Wit MJ, Ashwal LD* (eds) Greenstone belts. Oxford University Press, Oxford, pp 398–421
- Perchuk LL* (1969) The effect of temperature and pressure on the equilibria of natural Fe-Mg minerals. *Intern Geol Rev* 11(8): 875–901
- Perchuk LL* (1973) Thermodynamic regime of deep-seated petrogenesis. Nauka Press, Moscow, 300 p (in Russian)
- Perchuk LL* (1976) Gas-mineral equilibria and possible geochemical model of the Earth's Interior. *Physics Earth Planet Int* 13: 232–239
- Perchuk LL* (1977) Thermodynamic control of metamorphic processes. In: *Saxena SK, Bhattacharji S* (eds) Energetics of geological processes. Springer, New York, pp 285–352
- Perchuk LL* (1989) *P-T*-fluid regimes of metamorphism and related magmatism with specific reference to the Baikal Lake granulites. In: *Daly JS, Yardley BWD, Cliff BR* (eds) Evolution of metamorphic belts. Geol Soc London Spec Publ 42: 275–291
- Perchuk LL* (1991) Studies in magmatism, metamorphism, and geodynamics. *Int Geol Rev* 33: 311–374

- Perchuk LL, Gerya TV* (1995) Studies of the boundaries between granulite facies terranes and cratons. Centennial Geocongress, Extended Abstracts II. Geol Soc S Afr, Johannesburg, pp 622–623
- Perchuk LL, Krotov AV* (1998) Petrology of the mica schists of the Tanaelv belt in the southern tectonic framing of the Lapland granulite complex. *Petrology* 6(2): 149–179
- Perchuk LL, Aranovich LYa, Podlesskii KK, et al* (1985) Precambrian granulites of the Aldan shield, eastern Siberia, USSR. *J Metam Geol* 3: 265–310
- Perchuk LL, Gerya TV, Nozhkin AD* (1989) Petrology and retrogression in granulites of the Kanskiy Formation, Yenisey Range, Eastern Siberia. *J Metam Geol* 7: 599–617
- Perchuk LL, Podladchikov YuYu, Polaykov AN* (1992) *P-T* paths and geodynamic modeling of some metamorphic processes. *J Metam Geol* 10: 311–319
- Perchuk LL, Gerya TV, van Reenen DD, et al* (1996) The Limpopo metamorphic complex, South Africa 2. Decompression/cooling regimes of granulites and adjusted rocks of the Kaapvaal craton. *Petrology* 4(6): 571–599
- Perchuk LL, Gerya TV, van Reenen DD, Smit CA* (1997) Cratonization: from greenstone belts to granulites. *EUG 9 [Abstr Suppl 1] to Terra Nova* 99: 362
- Perchuk LL, Krotov AV, Gerya TV* (1999a) Petrology of amphibolites of the Tanaelv Belt and granulites of the Lapland complex. *Petrology* 7(4): 539–563
- Perchuk LL, Gerya TV, Van Reenen DD, et al* (2000) *P-T* paths and tectonic evolution of shear zones separating high-grade terrains from cratons: examples from Kola Peninsula (Russia) and Limpopo Region (South Africa). *Mineral Petrol* (this issue)
- Pozhilenko VI, Smolkin VF, Sharov NV* (1997) Seismic-geological models for the Earth's crust in the Lapland-Pechenga region, Russia. In: *Sharov NV* (ed) A seismological model of the lithosphere of northern Europe: Lapland-Pechenga Region. Russ Acad Sci, Kola Sci Center, Apatity, pp 181–208 (in Russian)
- Petrova ZI, Levitskii VI* (1984) Petrology and geochemistry of granulite complexes of the Baikal Lake region. Nauka Press, Moscow, 295 p
- Przhjalgovskiy E, Terekhov E* (1995) Karasjok-Belomorian parautochton (2.2–1.9 Ga) and some aspects of structural and geochemical reworking of rock complexes. *Nor Geol Unders, Spec Publ* 7: 193–200
- Raith M, Raase P, Hormann PK* (1982) The Precambrian of Finnish Lapland: evolution and regime of metamorphism. *Geol Rdsch* 71: 230–244
- Ramberg H* (1981) Gravity, deformation and geological application. Academic Press, New York, 399 p
- Ridley J* (1992) On the origins and tectonic significance of the charnockite suite of the Archean Limpopo Belt, NMZ, Zimbabwe. *Precamb Res* 55: 407–427
- Robertson IDM* (1973) Potash granites of the southern edge of the Rhodesian Craton and the Northern Granulite Zone of the Limpopo mobile belt. Symposium on granites, gneisses and related rocks. *Geol Soc S Afr, Spec Publ* 3: 265–276
- Robertson IDM* (1974) Explanation for the geological map of the country south of Chibi. Short Reports, *Geol Surv Rhodesia* 41: 40
- Robertson IDM, Du Toit MC* (1981) The Limpopo Belt. In: *Hunter DR* (ed) Precambrian of the Southern Hemisphere. Elsevier, Amsterdam, pp 641–671
- Roering C, van Reenen DD, Smit CA, et al* (1992a) Tectonic model for the evolution of the Limpopo Belt. *Precamb Res* 55(1–4): 539–552
- Roering C, van Reenen DD, de Wit MJ, et al* (1992b) Structural geological and metamorphic significance of the Kaapvaal Craton–Limpopo Belt contact. *Precamb Res* 55(1–4): 69–80
- Roering C, van Reenen DD, Smit CA, Du Toit R* (1995) Deep crustal embrittlement and fluid flow during granulite metamorphism in the Limpopo Belt, South Africa. *J Geol* 103: 673–686

- Rollinson HR* (1993) A terrain interpretation of the Archean Limpopo Belt. *Geol Mag* 130: 755–765
- Rollinson HR* (1997) Plumes, underplating and cratonization. *EUG 9 [Abstr Suppl 1]* to *Terra Nova* 9: 362
- Rollinson HR, Blenkinsop TG* (1995) The magmatic, metamorphic and tectonic evolution of the NMZ of the Limpopo Belt in Zimbabwe. *J Geol Soc Lond* 152: 65–75
- Sharkov EV, Lyahovich VV, Ledneva GV* (1994) Petrology of Early Proterozoic coronitic complex from the White island, Pezhostrov, northern Karelia. *Petrology* 2(5): 511–531
- Thompson AB* (1990) Heat, fluids, and melting in the granulite facies. In: *Vielzeuf D, Vidal Ph* (eds) *Granulites and crustal evolution*. Kluwer, Dordrecht, pp 37–58 (NATO ASI Series C)
- Tomkeieff SI* (1983) *Dictionary of petrology*. John Wiley and Sons, New York, 350 p
- Tsunogae T, Miyano T, Ridley J* (1992) Metamorphic P-T profiles from the Zimbabwe Craton to the Limpopo Belt, Zimbabwe. *Precamb Res* 55(1–4): 259–277
- van Reenen DD* (1986) Hydration of cordierite and hypersthene and a description of the retrograde orthoamphibole isograd in the Limpopo belt, South Africa. *Am Mineral* 71: 900–915
- van Reenen DD, Smit CA* (1996) The Limpopo metamorphic complex, South Africa 1. Geological setting and relationships between the granulite complex and the Kaapvaal and Zimbabwe cratons. *Petrology* 4(6): 562–570
- van Reenen DD, Roering C, Brandl G, et al* (1990) The granulite facies rocks of the Limpopo belt, southern Africa. In: *Vielzeuf D, Vidal Ph* (eds) *Granulites and crustal evolution*. Kluwer, Dordrecht, pp 257–289 (NATO ASI Series C)
- van Reenen DD, McCourt S, Smit CA* (1995) Are the Southern and Northern Marginal Zones of the Limpopo Belt related to a single continental collisional event? *S Afr J Geol* 98: 489–504
- van Schalkwyk JF, van Reenen DD* (1992) High-temperature hydration of ultramafic granulites from the Southern Marginal Zone of the Limpopo Belt by infiltration of CO₂-rich fluid. *Precamb Res* 55: 337–352
- Vinogradov VA, Bogdanova MN, Efimov MM* (1980) *Granulite belt of the Kola Peninsula*. Nauka Press, Leningrad, 208 p (in Russian)

Authors' addresses: *L. L. Perchuk, A. V. Krotov, and M. Yu. Shur*, Department of Petrology, Geological Faculty, Moscow State University, Vorobievsky Gory, Moscow, 119899 Russia, e-mail: llp@geol.msu.ru; llp@p1854.home.chg.ru; *T. V. Gerya and O. G. Safonov*, Institute of Experimental Mineralogy, Russian Academy of Sciences, Chernogolovka, Moscow district, 142432 Russia, e-mail: taras@iem.ac.ru; *D.D. van Reenen and A. Smit*, Department of Geology, Rand Afrikaans University, Auckland Park, South Africa, e-mail: ddvr@na.rau.ac.za

Appendix 1: Abbreviations of geological units and symbols of mineralsTable A1-1. *Symbols of minerals used*

Symbol	Mineral	Symbol	Mineral	Symbol	Mineral
<i>Alm</i>	almandine	<i>Grs</i>	Grossular	<i>Prp</i>	pyrope
<i>Ap</i>	apatite	<i>Ilm</i>	ilmenite	<i>Qtz</i>	quartz
<i>And</i>	andalusite	<i>Kfs</i>	K-feldspar	<i>Sc</i>	scapolite
<i>Bt</i>	biotite	<i>Ky</i>	kyanite	<i>Sil</i>	sillimanite
<i>Chl</i>	chlorite	<i>Mag</i>	magnetite	<i>Sph</i>	sphene
<i>Crd</i>	cordierite	<i>OK*</i>	AlAlO ₃	<i>Spl</i>	spinel
<i>Ep</i>	epidote	<i>Opx</i>	orthopyroxene	<i>Tur</i>	turmaline
<i>East</i>	eastonite	<i>Phl</i>	phlogopite	<i>Ru</i>	rutile
<i>Grt</i>	garnet	<i>Pl</i>	plagioclase	<i>Zc</i>	zircon

*OK orthocorundum (*Aranovich and Podlesskii, 1989*)

Table A1-2. *Abbreviations for major geological units*

Abbreviations	Full name	Isotopic age, Ga
GSB	Greenstone Belt	
HGT	High grade terrains:	
	Lapland HGT	1.9–1.85
	Limpopo HGT	~ 2.63
KVC	Kaapvaal Craton	> 2.75
ZC	Zimbabwe Craton	> 2.8
HRSZ	Hout River Shear Zone (Limpopo area)	2.63
CZ	Central Zone of the Limpopo HGT	~ 2.6 ⇒ ~ 2.0
NMZ	North Marginal Zone of the Limpopo HGT	2.63
SMZ	South Marginal Zone of the Limpopo HGT	2.63
KB	Kola Central Block	2.9–2.65
PC	Pechenga Complex	2.46–1.85
MB	Murmansk Block	2.9–2.45
KC	Karelian craton	3.1–2.7
BC	Belomorian Complex of the Karelian craton	> 2.8
IC	Inari Craton	> 2.8
TB	Tanaelv (Tana) Belt separating of the Lapland HGT from the BC	2.46–1.9
KTG	Korva Tundra Group of the TB	1.9
KG	Kandalaksha group of the TB	2.46–1.9
NSZ	Northern Shear Zone separating of the Lapland HGT from the Inari craton and KB	no data

Appendix 2: Two examples showing how a *P-T* path was deduced*Thermodynamic symbols used in Appendix 2*

X_i molar fraction of the component i (for example, $X_{Mg} = Mg/Mg + Fe$); N_i 100 X_i , molar per cent of the component i ; a_i activity of the component i ; T temperature, K;

P pressure, kbar; G Gibbs free energy, cal/mole; S entropy, cal/mole/K; V volume, cal/bar; H enthalpy, cal; R 1.987 cal/mole/K, ΔS_T^0 , ΔH_T^0 , ΔV_T^0 = change in corresponding standard parameters of a reaction at standard temperature T .

Thermodynamic data used in Appendix 2

All internally consistent thermodynamic data and activity models for the end-members of mineral solid solutions are given in Table A2-1 and Table A2-2, respectively. *Bulk compositions* of metapelites used in Appendix 2 are given in Table A2-3.

Sample DR45 (Table 2)

This sample represents a coarse-grained *Grt-Opx* metapelite (see Fig. 1b). The rock is characterized by a relatively low degree of consumption of the primary Mg-rich garnet porphyroblasts. Cores of the isometric 2–4 mm garnet contain elongated oriented inclusions of plagioclase and quartz. The orientation of these inclusions in different garnet grains is identical and consistent with the orientation of elongated 1–3 mm grains of primary *Opx_{Al}* in the *Qtz-Pl* matrix. Compositions of the garnet cores are characterized by flat profiles (e.g., Fig. 6a) not affected by late diffusion and re-crystallization. The garnet porphyroblasts are rimmed by the late 100–1000 μm wide *Opx-Crd* corona textures. In places, cordierite of $N_{\text{Mg}} = 84$ forms separate grains within the corona textures.

Table A2-1 An internally consistent thermodynamic data set used for geothermobarometry and calculations of garnet isolines in P - T diagrams (after Perchuk et al., 1985, 1996; Aranovich and Podlesskii, 1989; Gerya and Perchuk, 1990)

No.	Reaction	ΔH_{970}^0 , cal	ΔS_{970}^0 , e.u.	ΔV_{970}^0 , cal/bar
r1	$1/3Prp + 2/3Sil + 5/6Qtz = 1/2Crd_{\text{Mg}}$	51	4.620	0.63827
r2	$1/3Prp + 1/2Crd_{\text{Fe}} = 1/3Alm + 1/2Crd_{\text{Mg}}$	-6134	-2.668	-0.03535
r3	$1/2Crd_{\text{Mg}} = En + 3/2Qtz + OK$	6096	-4.897	-0.43628
r4	$1/3Crd_{\text{Mg}} + Fs = 1/2Crd_{\text{Fe}} + En$	1368	0.014	0.011930
r5	$Prp + 3/2Qtz = 2En + 1/2Crd_{\text{Mg}}$	-3311	3.028	0.76483
r6	$1/3Prp + 1/3Bt_{\text{Fe}} = 1/3Alm + 1/3Bt_{\text{Mg}}$	-7843	-5.699	0.0250
r7	$Prp + Kfs + H_2O = Phl + Sil + 2Qtz$	-23595	-31.214	0.547
r8	$1/3Grs + 2/3Sil + 1/3Qtz = An$	2722	10.266	0.435
r9	$1/2Grs + Prp + Kfs + H_2O = Phl + 3/2An + 3/2Qtz$	-19512	-15.815	1.1995

Table A2-2. Activities of some end members of garnet, cordierite and orthopyroxene which participate in reactions of Table A2-1

Garnet (Aranovich and Podlesskii, 1989)–

$$RT \ln a_{Prp}^{Grt} = 3RT \ln X_{Mg}^{Grt},$$

$$RT \ln a_{Alm}^{Grt} = 3RT \ln X_{Fe}^{Grt},$$

where $X_{Mg}^{Grt} = Mg/(Fe + Mg)$, $X_{Fe}^{Grt} = Fe/(Fe + Mg)$.

Cordierite (Gerya and Perchuk, 1990)–

$$RT \ln a_{Crd-Mg} = 2RT \ln X_{Mg}^{Crd} - 1333 + 0.617T - 0.336P + 1026(1 - X_{H_2O}) + 472(1 - X_{H_2O})^2,$$

$$RT \ln a_{Crd-Fe} = 2RT \ln X_{Fe}^{Crd} - 1333 + 0.617T - 0.336P + 1026(1 - X_{H_2O}) + 472(1 - X_{H_2O})^2,$$

where $X_{Mg}^{Crd} = Mg/(Fe + Mg)$; $X_{Fe}^{Crd} = Fe/(Fe + Mg)$; $X_{H_2O} = H_2O/(H_2O + CO_2)$ –mole fraction of water in metamorphic fluid; for all calculations, $X_{H_2O} = a_{H_2O} = 0.2$ estimated for the Limpopo and Lapland granulites was accepted, see text.

Orthopyroxene (Aranovich and Podel'sskii, 1989)–

$$RT \ln a_{En} = RT \ln X_{En} + (X_{Fs})^2(1.86T - 2533) + X_{Fs}X_{OK}(2671 + 1.86T) - (1237 + 0.1425P)(X_{OK})^2;$$

$$RT \ln a_{Fs} = RT \ln X_{Fs} + (X_{En})^2(1.86T - 2533) + X_{En}X_{OK}(1.86T - 7937) - (6441 + 0.1425P)(X_{OK})^2;$$

$$RT \ln a_{OK} = RT \ln X_{OK} - 6441(X_{Fs})^2 - X_{En}X_{Fs}(6145 + 1.86T) - 1237(X_{En})^2 - 0.1425P(1 - X_{OK})^2,$$

where $X_{En} = Mg/(Fe + Mg + Al/2)$; $X_{Fs} = Fe/(Fe + Mg + Al/2)$; $X_{OK} = Al/(2Fe + 2Mg + Al)$.

Table A2-3. Bulk compositions of some Limpopo high-grade metapelites used for mass-balance calculations

Sample	DR19	DR45	DV3	LW7	BY27	BY30
SiO ₂	56.85	48.79	65.30	56.92	66.17	48.13
TiO ₂	0.87	0.98	0.68	0.85	0.83	2.55
Al ₂ O ₃	20.04	19.28	13.70	17.80	13.82	23.70
Fe ₂ O ₃	1.25	2.18	0.69	9.29	1.25	2.90
FeO	7.14	10.61	7.30	4.17	7.23	12.97
MnO	0.06	0.14	0.00	0.07	0.08	0.12
MgO	6.86	9.44	6.30	8.95	6.65	4.86
CaO	0.78	1.86	1.39	1.61	1.16	0.26
Na ₂ O	1.26	1.68	1.80	2.20	0.95	0.24
K ₂ O	2.67	2.04	1.82	1.46	1.87	3.40
Total	97.78	97.00	98.98	103.32	100.01	99.13

Chemical parameters of garnet, orthopyroxene and cordierite and P-T parameters of their equilibria

The garnet cores (see Fig. 6a) from the primary $Qtz + Grt + Opx_{Al}$ assemblage show distinct variations in their compositions, whereas the Al-rich orthopyroxene and newly formed-cordierite are uniform (Table 3). This leads to the highest P-T estimates corresponding to the core compositions of garnet, orthopyroxene, and

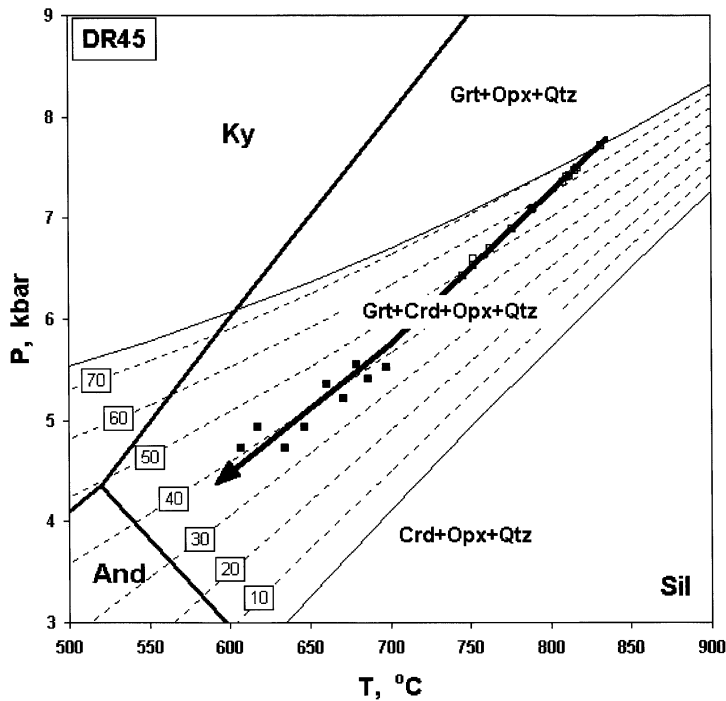


Fig. A1. Thermodynamic evolution of Sample DR45 from the Limpopo HGT. Isolines of the garnet content in the assemblage $Grt + Opx + Crd + Qtz$ (dashed lines) are calculated on the basis of bulk composition of the rock (Table A2-3) and thermodynamic data of Table A2-1. Solid symbols define P - T parameters calculated for rims of contacting minerals, while open symbols reflect those for cores

cordierite, with the upper portion of the P - T path being parallel to the isopleth of $N_{Mg}^{Crd} = 85$ (Fig. 6b). These parameters probably reflect the first stage of the decompression cooling from the peak metamorphic conditions.

The P - T parameters of the second stage of retrogression were calculated from the rim compositions (Table 3) of contacting minerals inside of the corona textures of sample DR45. This stage is indicated by the lower portion of the P - T path in Fig. 6b where a decrease in P and T leads to a decrease in N_{Mg}^{Grt} and N_{Al}^{Opx} at about constant N_{Mg}^{Crd} and N_{Mg}^{Opx} .

The P - T path that is drawn with the described “point-to-point” method reflects a significant decompression cooling of sample DR45. In combination with the mass-balance calculations, this path allows estimation of the garnet consumption degree using the bulk rock composition from Table A2-3. Figure A1 demonstrates the relationship between the P - T path and calculated isolines of the garnet content normalized to 100%: the content of garnet in the rock decreases from ~ 70 to $\sim 40\%$ that corresponds to 40% of the highest possible garnet consumption, i.e. $100 \cdot (70-40)/70 = 40\%$. This is in accord with replacement of about 30% of garnet by the Crd - Opx symplectites observed in sample DR45. In addition, the upper end of the P - T trajectory in Fig. A1 falls on the line that separates the Opx - Grt - Qtz stability field from the Crd - Opx - Grt - Qtz field, which is consistent with the absence of cordierite in the Qtz - Pl matrix.

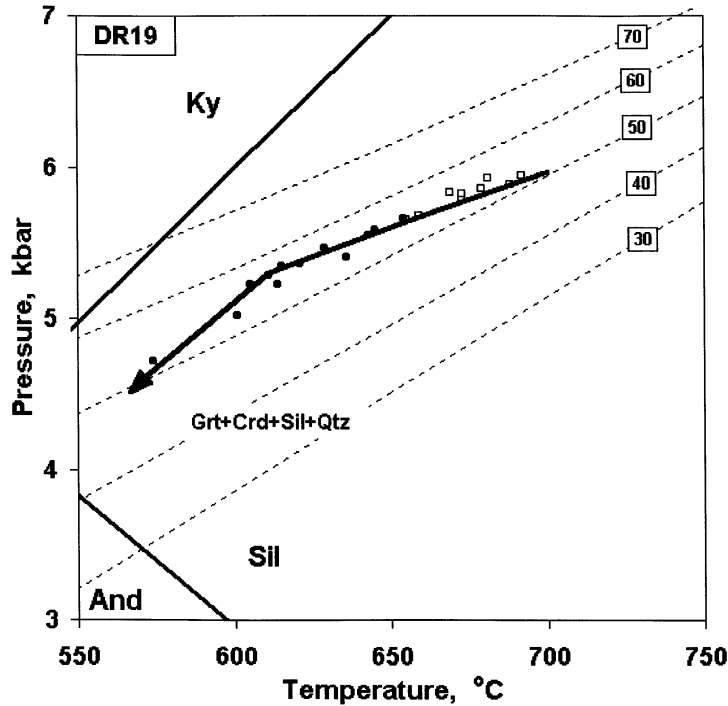


Fig. A2. Thermodynamic evolution of Sample DR19 from the Limpopo HGT. Isolines of garnet content in the assemblage *Grt + Sil + Crd + Qtz* (dashed lines) are calculated on the basis of bulk composition of the rock (Table A2-3) and thermodynamic data of Table A2-1. Solid symbols define *P-T* parameters calculated for rims of contacting minerals, while open symbols reflect those for cores

Sample DR19 (Table 2, Fig. 1b)

This sample is the coarse-grained porphyroblastic *Grt-Crd-Opx* metapelite that is characterized by the two microtexture assemblages formed during two subsequent stages of metamorphic evolution. The first stage is characterized by the *Crd-Opx* corona textures that must have formed around garnet, *Grt(1)*, in contact with quartz due to reaction (1). In contrast to sample DR45, the garnet porphyroblasts from these textures do not contain Mg- and Ca-rich cores, and thus, the *P-T* parameters of the earliest stage of metamorphism can not be calculated. The second stage is recorded in the delicate *Grt(2) + Qtz + Sil* intergrowths between *Grt* and cordierite (Fig. 9a) formed due to reaction (5). Figure 9a shows that *Grt(1)* and *Grt(2)* have similar $N_{Mg}^{Grt(1)} = 39-40$. In places, however, N_{Mg} of the *Grt(2)* unzoned isolated grains varies within 40–35. The Mg number of cordierite increases from the cores towards the contact with *Grt(2)* (Fig. 9a). Using compositions of the cores of *Grt(1)* and cordierite and applying thermodynamic data for reactions r1 and r2 from, the highest *P-T* parameters were calculated. Results of these calculations are given in Table 3 and shown as open rectangles in Fig. 9b. The lower *P-T* parameters were obtained using the rim composition of *Grt(2)* and *Crd*. The results are shown by filled rectangles in Fig. 9b, where the major portion of the *P-T* path reflects near-isobaric cooling of the rock.

Figure A2 demonstrates a systematic increase of the garnet content in the rock between 700° and 625 °C along the calculated *P-T* path.